Korean J. Chem. Eng., **31**(8), 1289-1305 (2014)
DOI: 10.1007/s11814-014-0156-6
pISSN: 0256-1115
eISSN: 1975-7220

INVITED REVIEW PAPER

Functionalization of magnetic nanoparticles for biomedical applications

Dung The Nguyen and Kyo-Seon Kim†

Department of Chemical Engineering, Kangwon National University, Chuncheon, Kangwon 200-701, Korea
(*Received 25 March 2014 • accepted 2 June 2014*)

Abstract−Interest in utilizing magnetic nanoparticles for biomedical treatments originates from their external controllability of transportation and movement inside biological objects and magnetic heat generation. Advances in nanoparticle and nanotechnology enable us to produce magnetic nanoparticles of specific morphology and to engineer particle surfaces to manipulate their characteristics for specific applications. Intensive investigations and developments have been carried out in improving the quality of magnetic particles, regarding their size, shape, size distribution, their magnetism and their surface. The magnetic nanoparticles with appropriate surface chemistry can conjugate various biomaterials such as drugs, proteins, enzymes, antibodies, or nucleotides to be used for numerous *in vivo* applications including MRI contrast enhancement, immunoassay, hyperthermia, drug delivery, and cell separation. Here we review both the key technical principles of magnetic nanoparticle synthesis and the ongoing advancement of biomedical treatments using magnetic nanoparticles, specifically, the advancement in controlled drug delivery and hyperthermia.

Keywords: Magnetic Nanoparticles, Controlled Synthesis, Biomedical Applications, Drug Delivery, Hyperthermia

INTRODUCTION

Magnetic Fe_3O_4 nanoparticles have been of great interest to worldwide researchers for biomedical applications. The Fe_3O_4 nanoparticles have their own advantages that provide many exciting opportunities in many applications, specifically, in the biomedical field. First, the particle size, shape and surface structure can be prepared controllably to match with the interest of study [1,2]. Second, the Fe_3O_4 nanoparticles play an important role as the contrast enhancement agents of magnetic resonance imaging due to their ability to capture the magnetic moment signal of protons around the magnetic nanoparticles [3,4]. Third, the Fe_3O_4 nanoparticles can be manipulated by an external magnetic force and this action at a distance provides tremendous advantages for many applications such as magnetic hyperthermia and targeted drug delivery as well as controlled drug release [5,6].

It is still a great challenge to synthesize Fe_3O_4 nanoparticles of customized size and shape. The Fe_3O_4 nanoparticles obtained under different synthetic conditions may display large differences regarding their magnetic properties due to formation of structural disorder and antiphase boundaries, or the existence of a magnetically dead layer at the particle surface. For biomedical treatments, the Fe_3O_4 nanoparticles should be highly homogeneous in size, shape and component. They also need to have sufficient magnetization, which ensures the external controllability. In colloidal form, the stability of Fe_3O_4 nanoparticles is of utmost importance. They must have good dispersion, stability and biocompatibility to prevent endocytosis by macrophages as well as to extend their residence time in circulating blood. Surface modifications and coatings can stabilize the magnetic Fe_3O_4 nanoparticles for better dispersion and biocompatibility. These can also provide functional surfaces for further modifications with various specific materials for diverse applications.

Herein, we will highlight the recent progress on the synthesis of various Fe_3O_4 nanostructures with growth mechanisms. We also provide a brief background on the physical properties of magnetic nanoparticles and then introduce design strategies for magnetic nanoparticles as a platform for controlled drug delivery and hyperthermia treatment. Furthermore, we will introduce and discuss some typical developments of mechanical actuation and manipulation of drug release which are important to accomplish high efficacy therapeutics in a noninvasive and remote fashion. Finally, we will discuss the physics and engineering of magnetic nanoparticles for hyperthermia treatment.

CONTROLLED SYNTHESIS OF Fe_3O_4 NANOPARTICLES

1. Size-controlled Synthesis of Fe_3O_4 Nanoparticles

Fe_3O_4 nanoparticles were widely synthesized through the co-precipitation of Fe^{2+} and Fe^{3+} aqueous solutions with a base. It has been reported that the particle size depended on the pH, temperature, Fe^{2+}/Fe^{3+} ratio and ionic strength of the medium [7-9]. A study on the ratio of Fe^{2+}/Fe^{3+} revealed that, only ratios between 0.4 and 0.6 produced monodisperse particles and, with the ratio of 0.5 which corresponds to magnetite stochiometry, the Fe_3O_4 nanoparticles were homogeneous in size and composition [10]. Since the Fe_3O_4 is not very stable and is sensitive to be oxidized and transformed into Fe_2O_3, the synthesis of Fe_3O_4 nanoparticles should be carried out in an oxygen-free environment by passing an inert gas [11]. The main advantage of the co-precipitation process is that a large amount of nanoparticles can be synthesized through the facile and moderate reaction conditions. However, this process has several disadvantages, such as limitation of size and shape uniformity, and poor dispersibility, which may induce greater nonuniformity in subsequent modi-

†To whom correspondence should be addressed.
E-mail: kkyoseon@kangwon.ac.kr

fication processes.

Monodisperse iron oxide nanoparticles were widely synthesized by hydrothermal and high-temperature reaction methods. Sun et al. [12,13] reported a synthesis of 4 nm monodisperse magnetite nanoparticles by refluxing a reaction mixture containing the iron (III) acetylacetonate, $Fe(acac)_3$, 1,2-hexadecanediol, oleic acid, and oleylamine in diphenyl ether solvent (boiling point of 265 °C), while 6-nm monodisperse Fe_3O_4 nanoparticles were obtained in benzyl ether solvent (boiling point of 300 °C). To make larger Fe_3O_4 nanoparticles, a seeded growth process was demonstrated for generating nanoparticles up to 16 nm by controlling the ratio of seed to additional precursor. A strategy using oleylamine as both reducing agent and stabilizer was developed to prepare monodisperse spherical Fe_3O_4 nanoparticles. [14] Jana et al. [15] reported the synthesis of monodisperse Fe_3O_4 colloidal nanoparticles of larger size via the pyrolysis of iron oleate salt. The iron oleate was mixed with octadecane and oleic acid, followed by heating to 300 °C. By changing the ratio of ferric oleate to oleic acid from 0.1 to 10, the diameter of the Fe_3O_4 nanoparticles could be controlled between 6 and 50 nm. Another study reported that triethylene glycol directly reacted with $Fe(acac)_3$ at an elevated temperature to prepare non-agglomerated Fe_3O_4 nanoparticles with uniform shape and narrow size distribution [16].

Hyeon's group prepared monodisperse iron oxide nanoparticles by thermal decomposition of an iron-oleate complex which was synthesized from pentacarbonyliron, $[Fe(CO)_5]$, and oleic acid, followed by controlled chemical oxidation with trimethylamine N-oxide as a mild oxidant [17]. Particle sizes of 4, 8, and 11 nm were obtained by using reaction mixtures of $[Fe(CO)_5]$ and oleic acid at molar ratios of 1 : 1, 1 :2 , and 1 : 3, respectively. In this synthesis, monodisperse iron nanoparticles were initially generated, and these were further oxidized controllably to produce iron oxide nanoparticles. By refluxing the mixtures generated from the combinations of the iron nanoparticles and the iron oleate complex, the monodisperse iron oxide nanoparticles with particle sizes from 6 nm to 15 nm were successfully prepared. The overall synthetic procedure was similar to seed-mediated growth as shown in Fig. 1 [18]. The ultra-large-scale synthesis of 40-g monodisperse Fe_3O_4 nanoparticles using inexpensive, nontoxic metal salts as reactants was reported [19]. In this process, Fe-oleate complex prepared from hydrated iron chloride and sodium oleate was transferred to an appropriate high-boiling-point solvent, and slowly heated to around 300 °C to produce the nanoparticles. The synthesis process was composed of two sequential steps: the thermal decomposition of iron-oleate complex to generate intermediate species, and the nucleation and growth of iron oxide nanoparticles from these intermediate species [20]. The particle size

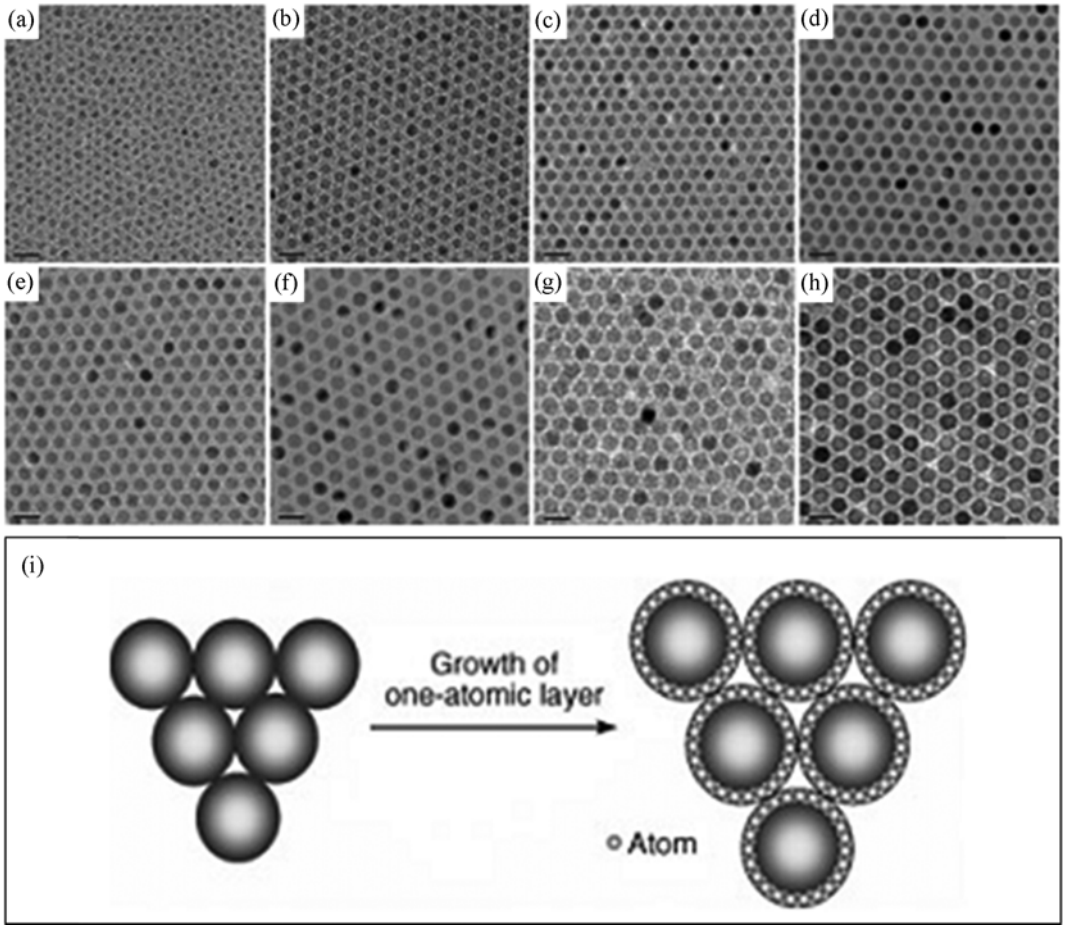

Fig. 1. TEM images of (a) 6-, (b) 7-, (c) 8-, (d) 9-, (e) 10-, (f) 11-, (g) 12-, and (h) 13-nm-sized air-oxidized iron oxide nanoparticles showing the one nanometer level increments in diameter and (i) schematic for direct and atomic-scale controlled synthesis of monodisperse nanoparticles [18].

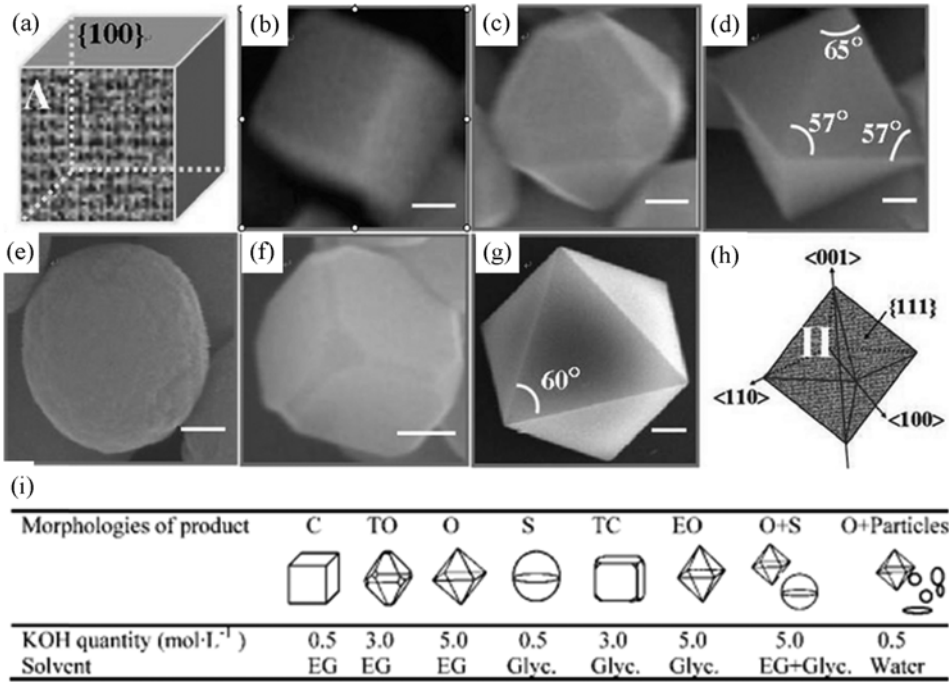

Fig. 2. Schematic illustration of (a) ideal cube structure and the evolution process from (b) cube to (c) truncated octahedra to (d) octahedra and from (e) sphere to (f) truncated octahedra to (g) equilateral octahedra, and (h) ideal octahedral structure (Scale bar=100 nm) and (i) synthesis conditions for the preparation of Fe_3O_4 nanoparticles with various morphologies (Cube (C), truncated octahedron (TO), octahedron (O), sphere (S), truncated cube (TC), equilateral octahedron (EO), ethylene glycol (EG), and glycerol (Glyc.)) [26].

could be controlled by using different solvents with different boiling points. For instance, 5-, 9-, 12-, 16-, and 22-nm-sized iron oxide nanoparticles were synthesized by using 1-hexadecene, octyl ether, 1-octadecene, 1-eicosene, and trioctylamine which has a boiling point of 274 °C, 287 °C, 317 °C, 330 °C and 365 °C, respectively.

Ge et al. [21] reported the synthesis of highly water dispersible Fe_3O_4 nanoparticles with uniform size from about 31 to about 174 nm. Each nanoparticle was composed of many primary smaller nanoparticles of approximately 10 nm in diameter. In their process, iron (III) chloride and diethylene glycol (DEG) were used as precursor and solvent, respectively. Poly(acrylic acid) was selected as surfactant. Introduction of NaOH into the hot mixture of DEG, $FeCl_3$, and PAA resulted in the hydrolysis of $FeCl_3$. Under the reductive atmosphere provided by DEG at high temperature, $Fe(OH)_3$ was partially transformed into $Fe(OH)_2$, and finally Fe_3O_4 nanoparticles were formed through dehydration. These Fe_3O_4 primary nanoparticles spontaneously aggregated to form larger-sized Fe_3O_4 nanoparticles. The size of the Fe_3O_4 nanoparticles could be precisely controlled by simply increasing the amount of NaOH, while keeping all other parameters fixed.

2. Shape-controlled Synthesis of Fe_3O_4 Nanoparticles

The crystal structure analysis revealed that Fe_3O_4 nanoparticles showed a face-centered cubic crystal structure, and the general sequence for the surface energies of magnetite structure was $\gamma\{111\} < \gamma\{100\} < \gamma\{110\}$ [22]. As a result, the Fe_3O_4 nuclei exhibited octahedral morphology with eight {111} planes. Swaminathan et al. [23] pointed out that the final particle shape was defined by the ratio of growth rate in the <100> direction to that in the <111> direction. Octahedral nanoparticles surrounded by eight {111} planes were generated when the growth rate along the <100> direction was faster than that along the <111> direction [24]. On the other hand, if the growth rate along the <111> direction was faster than that of the <100> direction, the nanoparticles would be bounded by {100} planes, resulting in the formation of nanocubes [25]. Fig. 2 shows the formation of Fe_3O_4 nanoparticles with specific morphologies, simply by changing the solvent system and amount of KOH. In a typical process, the $FeSO_4$ is dissolved in ethylene glycol or glycerol to form a homogeneous solution. Then, a KOH solution is quickly added into the solution at room temperature. The mixture is then transferred into a Teflon lined stainless steel autoclave, sealed, and maintained at 200 °C for 24 for the complete formation of product particles. The KOH concentration and solvent properties determine the growth rate along <100> direction to <111> direction, leading to the evolution of different particle morphologies [26].

Fe_3O_4 nanoprisms are synthesized through solvothermal or hydrothermal process, using $Fe(acac)_3$ as the Fe precursor, toluene as a solvent, and oleylamine as both surfactant as well as reducing agent [27]. The specific adhesion of oleylamine to the (111) facet plays an important role in synthesizing the nanoprisms. The high-indexed (220) facet was also observed to be exposed as the side face of the prisms. Other researchers synthesized Fe_3O_4 nanoprisms by using $FeCl_3 \cdot 6H_2O$ as the precursor, ethylene glycol (EG) as a solvent, 1,3-propanediamine (PDA) as a surfactant and CH_3COONa (NaAc) as an additive [28]. They found that the $-NH_2$ group in PDA is able to coordinate with Fe^{3+}, and thus, change the surface conditions of the Fe_3O_4 nanoparticles. Therefore, the morphology of Fe_3O_4 nanoprisms was controllable by varying the volume ratio between EG and PDA.

Palchoudhury et al. [29] synthesized highly crystalline Fe_3O_4 nanoworms via a modified "heat-up" method using iron oleate as the precursor in mixture of 1-octadecene and oleic acid as solvent. While heating the reactant mixture, a 1-octadecene solution containing trioctylphosphine oxide (TOPO) was injected into the mixture. The time-dependent studies suggested that these nanoworms were formed from the aggregation of individual nanospheres. The aggregation was induced by the high percentage coverage of a weakly bound ligand (trioctylphosphine oxide) on the iron oxide surfaces. The magnetic properties changed from superparamagnetic to ferromagnetic to transform the Fe_3O_4 shape from spheres to elongated nanoworms.

Formation of Fe_3O_4 nanoparticles with porous/hollow structures is expected to integrate the valuable characteristics of porous/hollow structure and unique magnetic property of Fe_3O_4 material in a single platform, which can provide opportunities to tune their properties for specific applications. The template synthesis is an effective and common method for synthesizing porous/hollow nanostructures. Preparation of porous/hollow structures by template synthesis method involves the functionalization of template surface to achieve favorable surface properties, deposition of shell materials or their precursors with subsequent treatments to form solid shells, and selective removal of the templates. For instance, the composite core-shell and hollow Fe_3O_4 nanospheres were prepared by adsorption/precipitation of Fe_3O_4 nanoparticles or Fe^{2+} precursor onto functionalized polystyrene templates [30,31]. The hollow core diameter was mainly determined by the diameter of the polymer templates, and the thickness of magnetite shell layer was controlled by either the number of adsorption/precipitation cycles performed or the concentration of Fe precursor.

The template itself could be involved as a reactant in the synthetic process of the shell material. It has been reported that the Fe_3O_4 hollow nanoparticles were successfully prepared though the controlled oxidation of the Fe nanoparticles as templates [32,33]. The Fe nanoparticles were not chemically stable, and would be oxidized to form Fe/Fe_3O_4 core/shell structures. Controlled oxidation of these core/shell nanoparticles led to the formation of hollow Fe_3O_4 nanoparticles, eventually. It has been proposed that the Kirkendall effect directed the controlled oxidation of Fe templates in which Fe metal diffused outward faster than oxygen did inward and Fe_3O_4 was formed at the metal-oxide interface rather than in the interior. The Fe tem-

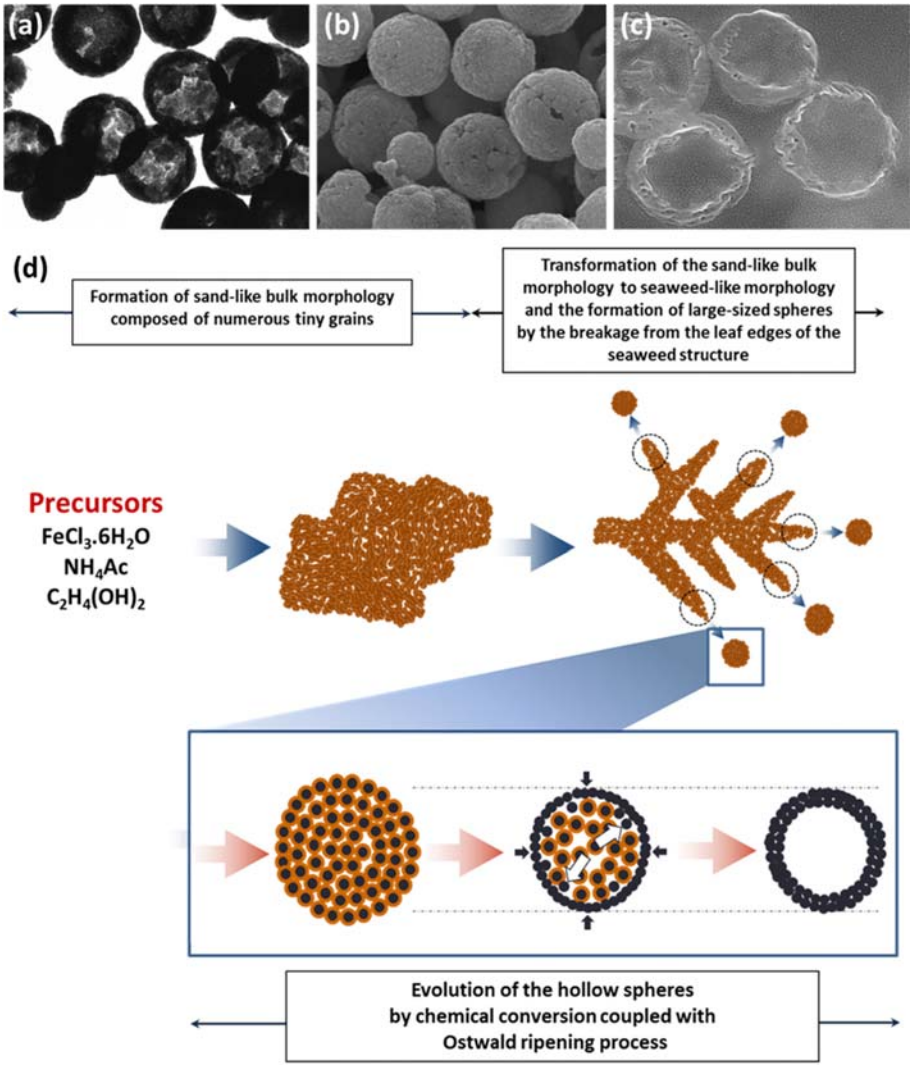

Fig. 3. (a) TEM and (b) SEM images for whole Fe_3O_4 porous/hollow nanoparticles. (c) SEM image for cross-sectional Fe_3O_4 porous/hollow nanoparticles. (d) Schematic of the particle formation and the hollow structure development through solvothermal process [46].

plate directly determined the shape and cavity size of the final hollow structure. This process was efficient, but it also required a complicated chemical and physical control for the formation of robust shells. For example, the specific geometry, diffusivity, and concentration profile of materials should satisfy the conditions by which the diffusivity of core material exceeds that of shell material [34]. For the Fe templates larger than the critical size of 8 nm, voids were not observed and only metal/metal oxide core/shell solid spheres were obtained [35]. Similar phenomena were observed for other materials such as Al, Cu and Zn [36,37].

Hollow nanocapsules of either haematite or magnetite are produced through a wrap-bake-peel process, depending on the heat treatment conditions [38,39]. Spindle-shaped akagenite (β-FeOOH) nanoparticles are prepared and then coated with a thin layer of silica by esterification of tetraethoxysilane in a base solution. The silica coated spindle is subject to a thermal treatment at 500 °C in air, leading to the formation of porous hollow nanocapsule structure with a rhombohedral haematite (α-Fe_2O_3). The haematite α-Fe_2O_3 is converted to magnetite Fe_3O_4 under a flow of hydrogen. Interestingly, the β-FeOOH nanorods and α-Fe_2O_3 nanocapsules are paramagnetic while the Fe_3O_4 nanocapsules are superparamagnetic at room temperature.

Recently, one template-free method to prepare Fe_3O_4 hollow nanoparticles has been developed based on the inside-out Ostwald ripening. Originally, the Oswald ripening referred to the growth of larger crystals from those of smaller size which have a higher solubility than the larger ones. Since this process involves matter relocation, it can occur within a crystallite aggregate for generation of interior space. The plausible mechanism is supported by several experimental observations. The dissolution-relocation of grains which built the aggregates could be rationalized by considering the different chelation modes between the outer and inner grains or by the existence of bubbles inside the aggregates [40-45]. Since the formation of hollow structure occurs simultaneously with the chemical conversion of solid material, the chemical conversion has been demonstrated as an important factor for the hollowing process [46]. The chemical conversions of solid material cause a little shrinkage of the grain size and thus make more voids between the grains inside the aggregates and lead to the formation of loose package of aggregates. The inner grains dissolve into the solution and then diffuse to the outer stable shell by the Ostwald ripening process, resulting in continuous expansion of cavity space inside the aggregates. Finally, the hollow structure is well developed with the complete chemical conversions of core grains. By simply adjusting the initial concentrations of Fe precursor and additive or varying other process variables such as processing time and temperature, the Fe_3O_4 porous/hollow nanoparticles are synthesized controllably with tunable particle size and porosity [47,48]. A schematic of the particle formation and hollow structure development of Fe_3O_4 porous/hollow nanoparticles is given in Fig. 3.

MAGNETISM OF Fe_3O_4 NANOPARTICLES

The properties of magnetic materials are characterized by the alignment of atomic magnetic moments generated by the spinning of electrons. This interaction gives rise to the macroscopic magnetic behaviors which are usually measured by magnetization (M), coercivity (H_C), and magnetocrystalline anisotropy constant (K). A large magnetic material usually consists of a number of domains in order to minimize its internal energy [49]. When an external magnetic field of strength, H, is applied to a multidomain magnetic particle, the magnetization, M, increases with H until a saturation value, M_S, is reached. Because the magnetic domains do not return to their original orientations when H is decreased after attaining the saturation magnetization, the magnetization displays a hysteresis loop, showing a remnant magnetization, M_R, of material when H returns to zero. The M_R can only be removed by applying a coercive field, H_C, in the opposite direction to the initially applied field. The coercivity is strictly related to the magnetocrystalline anisotropy constant (K), which reflects the energy required to change the direction of magnetic moments [50].

Magnetic parameters can be finely tuned by decreasing their size. When the particle size decreases to a certain level, the formation of a domain wall inside a magnetic particle is not thermodynamically favored, and thus the particle consists of only one magnetic domain with all of the spins aligned in the same direction [51]. If the magnetic anisotropy is stable enough, a typical hysteresis loop will be observed like a multidomain ferromagnet. On the contrary, if the thermal energy due to the rotation of single domain particle is large enough to overcome the anisotropy energy, the magnetization is no longer stable and returns to zero upon the removal of the applied magnetic field. This material is called as superparamagnetic material. The critical size for single domain structure which determines whether it is favorable to be multidomain or single domain and the critical size for superparamagnetic behavior which determines whether it shows the typical hysteresis loop or not could be predicted as shown in Fig. 4 [52].

Due to the external controllability, the magnetic nanoparticles

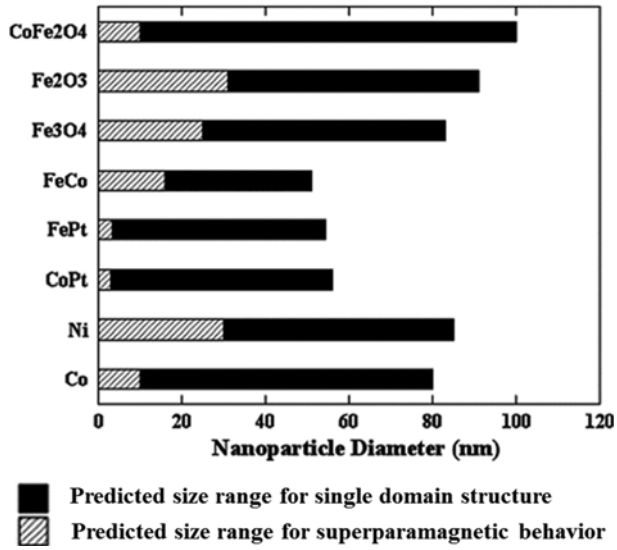

Fig. 4. Predicted size ranges for single domain structure and superparamagnetism behavior of common magnetic materials. For particles with diameter (D) larger than maximum diameter for single domain structure (D_{sd}), ($D>D_{sd}$), the magnetic materials split into multiple domains; for particles with diameter smaller than maximum diameter for superparamagnetism behavior (D_{sp}), ($D<D_{sp}$), they exhibit superparamagnetism; and for particles with diameter in between ($D_{sp}<D<D_{sd}$), they are single domain and ferromagnetic [52].

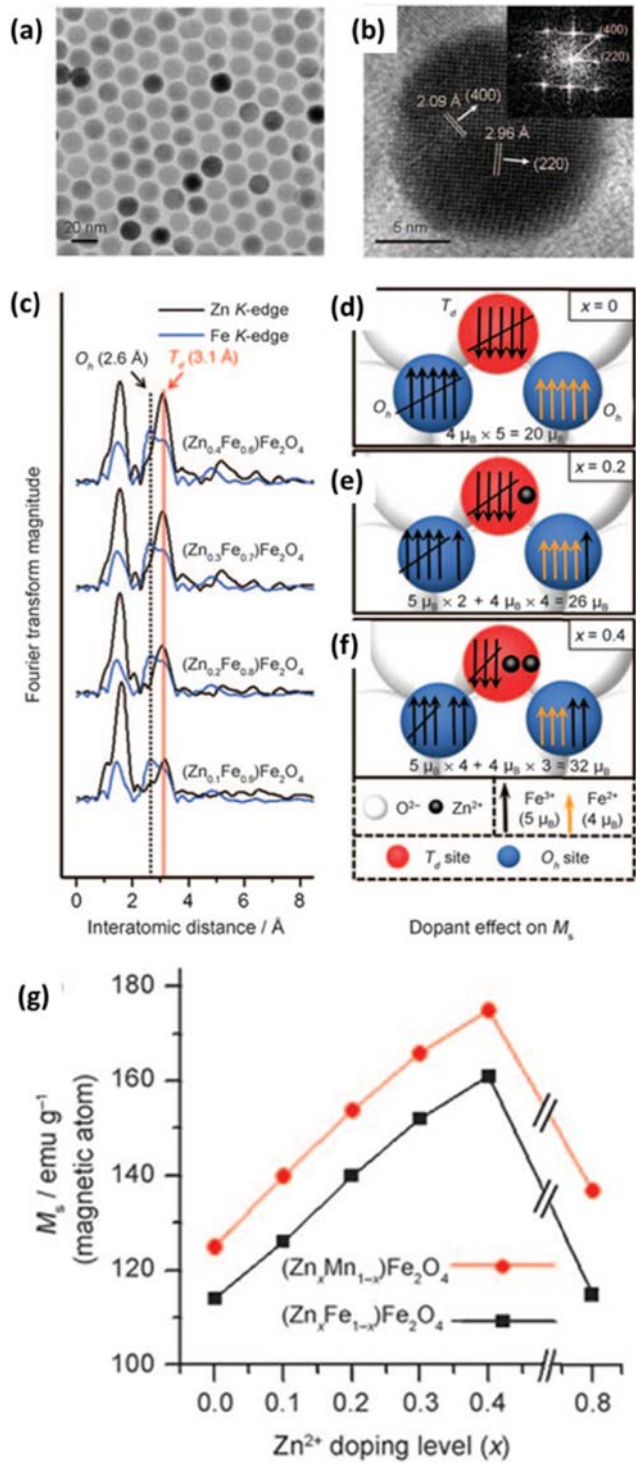

Fig. 5. (a) TEM image and (b) High-resolution TEM image of 15 nm $(Zn_{0.4}Fe_{0.6})Fe_2O_4$ nanoparticles. (c) Zn K edge EXAFS spectra of $(Zn_xFe_{1-x})Fe_2O_4$ nanoparticles (x=0.1, 0.2, 0.3, and 0.4). The intensity of the peak at 3.1 Å (red line) gradually becomes stronger as the Zn^{2+} doping level is increased, which indicates that the amounts of Zn^{2+} ions in T_d sites progressively increase. (d) Undoped, (e) Zn^{2+} doped (x=0.2), and (f) Zn^{2+} doped (x=0.4) magnetic spin alignment diagrams in spinel-structured $(Zn_xFe_{1-x})Fe_2O_4$ nanoparticles under an applied magnetic field. (g) Graphs of Ms versus Zn^{2+} doping level of $(Zn_xM_{1-x})Fe_2O_4$ (M=Mn^{2+}, Fe^{2+}) nanoparticles [63].

are potentially useful in areas such as magnetic resonance imaging, magnetic hyperthermia, drug delivery and bioseparation. The relationship of magnetic parameters to MRI sensitivity, heat generation, and magnetic attraction force has been reported and reviewed [4,53,54]. To optimize the properties of magnetic nanoparticles for biomedical applications, it is essential to consider the change of magnetic characteristics in the presence of various biocompatible coating or suspension media. Surface modification of the iron oxide nanoparticles with a non-magnetic shell usually led to the decrease in magnetization, which could be attributed to different mechanisms such as the weight contribution of non-magnetic material, the existence of a magnetically dead layer on the particle's surface and/or the existence of canted spins [55-57]. Since the magnetic response of a system to the surface modification is complex and system-specific, no correlation has been clearly established. For instance, LaConte et al. [58] found that as the coating thickness of the iron oxide nanoparticles increases, there is a dramatic decrease in R_2 relaxivity of the nanoparticles, while Duan et al. [59] reported that coating the superparamagnetic iron oxide nanoparticles with polyethylenimine could enhance the R_2 relaxivity of those nanoparticles.

Considering that the effects of magnetic nanoparticles for biomedical applications are strongly dependent on their magnetic characteristics, it is important to synthesize monodisperse nanoparticles with high saturation magnetization values. A metal dopant of ferrite nanoparticles has been pursued to achieve high and tunable nanomagnetism [13,60-62]. Jang et al. [63] synthesized Zn^{2+} doped ferrite nanoparticles by thermal decomposition of a metal chloride (MCl_2, M=Zn^{2+}, Mn^{2+}, and Fe^{2+}) and Fe(acac)$_3$ as shown in Fig. 5. The Zn^{2+} doping level was carefully controlled by varying the initial molar ratio of the metal chloride precursors. The magnetization saturation gradually increased as the Zn^{2+} doping level of nanoparticles increased from x=0 to 0.1, 0.2, 0.3, and 0.4. The magnetization saturation reached maximum for x=0.4. Structure investigation revealed that Zn^{2+} dopant mainly occupied tetrahedral sites of the spinel matrix. When x<0.4, Zn dopant induced the partial removal of antiferromagnetic coupling interactions between Fe^{3+} ions in the tetrahedral and octahedral sites. For higher Zn^{2+} doping levels (x>0.4), antiferromagnetic interaction of Fe^{3+} at nearby octahedral sites were dominant and the net magnetization moment decreased. According to the results, the Zn doped nanoparticles exhibited an eight- to fourteen-fold increase in MRI contrast and a fourfold enhancement in hyperthermic effects compared to the commercial Feridex nanoparticles from DaeJoon Pharmaceutical Co.

A magnetic coating on a magnetic nanoparticle has a dramatic influence on the magnetic properties by giving exchange across the interface between two different magnetic materials [64]. Recently, Yoon et al. [65], presented the formation of nanoparticles consisting of an elemental iron (Fe) core and an artificial ferrite shell (Fe@MFe_2O_4, M=Fe, Mn, Co) with a unique magnetization mechanism as shown in Fig. 6. The Fe cores were prepared by thermally decomposing iron complex [$Fe(CO)_5$] in the presence of oleylamine under air-free conditions. By adding Fe-oleate complexes and co-injecting Mn-oleate or Co-oleate complexes with Fe-oleate to Fe nanoparticles suspension and annealing the mixture at elevated temperatures, Fe nanoparticles with protective shells of the ferrite structure (Fe@Fe_3O_4, Fe@$MnFe_2O_4$ or Fe@$CoFe_2O_4$) were obtained. The core-sell nanoparticles displayed a hysteresis loop with high saturation magneti-

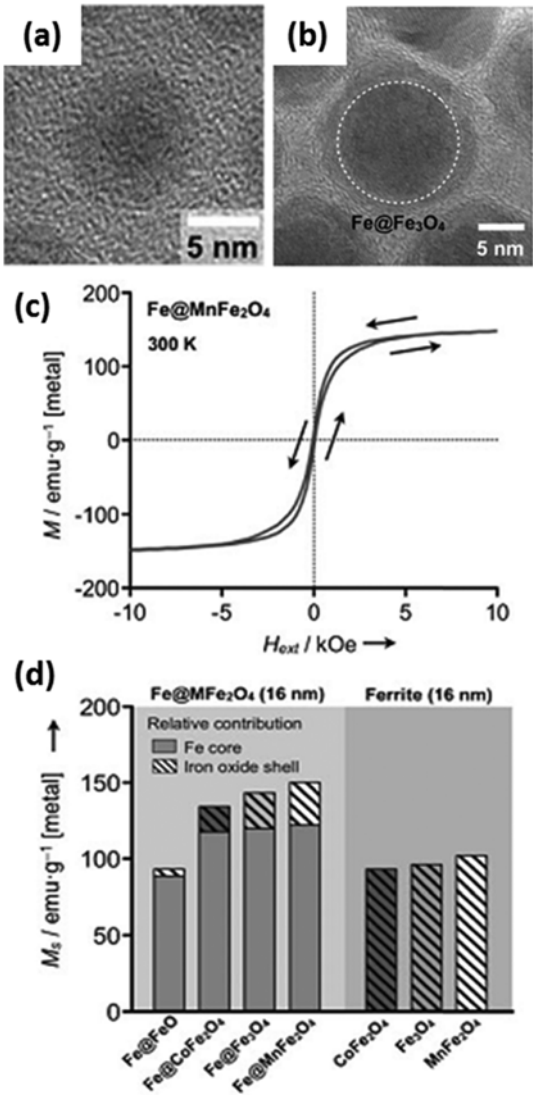

Fig. 6. (a) TEM images of a single Fe nanoparticles. (b) Fe nanoparticles were encased with crystalline ferrite to provide robust protection from oxidation ($Fe@Fe_3O_4$). TEM images confirmed that Fe nanoparticles (dotted circles) were preserved during the coating process. (c) The field-dependent magnetization (M) of $Fe@MFe_2O_4$ nanoparticles at 300 K showed an unusual feature for nanoparticles: negligible remanent moments but the presence of hysteresis. (d) All $Fe@MFe_2O_4$ MNPs (d=16 nm) had higher Ms than similarly sized ferrite nanoparticles [65].

zation but negligible coercivity and remanence. Consequently, their magnetic dipole interaction was negligible, resulting in good colloidal stability in aqueous media after suitable surface treatments. Increasing the crystallinity of ferrite shells could further improve the magnetization of such core-shell nanoparticles [66].

DESIGN AND SURFACE MODIFICATION OF Fe_3O_4 NANOPARTICLES FOR BIOMEDICAL APPLICATIONS

The biomedical applications of magnetic nanoparticles depend on a number of factors related to the size, shape and magnetism of the biocompatible nanoparticles as well as the physicochemical properties of the drug-loaded nanoparticles, field strength and geometry, depth of target tissue, rate of blood flow and so on. Surface coating of Fe_3O_4 nanoparticles is required to protect particle agglomeration and to provide functional groups for the conjugation of other materials such as drugs, targeting ligands, proteins and DNA sequences. Additionally, surface coating of Fe_3O_4 nanoparticles enhances nanoparticle pharmacokinetics, endosomal release, and tailored drug loading and release behaviors. To serve these coating functions, a diverse group of materials have been investigated including inorganic materials such as gold, silica, and organic materials such as dextran, chitosan, poly(ethylene glycol) and so on [67-69].

Fe_3O_4 nanoparticles can be stabilized by surface coating *in situ* by choosing the stabilizing agents to protect particle aggregation. For example, Fe_3O_4 nanoparticles covered by monocarboxyl-terminated poly(ethylene glycol) (MPEG-COOH) have been prepared as small as 4 nm and 9.8 nm directly through a one-pot process [70]. The MPEG-COOH molecules are covalently bound to the surface of the magnetite nanoparticles. The solubility of Fe_3O_4 nanoparticles increases with increasing molecular weight of polyethylene glycol. Another study reported that superparamagnetic Fe_3O_4 nanoparticles with a size of about 5.8 nm have been prepared by controlled coprecipitation of Fe^{2+} and Fe^{3+} in the presence of highly hydrophilic poly(vinylalcohol phosphate) [71]. Another typical example for the *in situ* coating of the Fe_3O_4 nanoparticles could be addressed to the development of superparamagnetic iron oxide nanoparticles-alginate system based on the gelation of alginate and iron salt precursor, the hydroxide formation of iron precursor by alkaline treatment, and the conversion to oxide [72-75].

Compared with the *in situ* coating, the post-synthesis coating has been used more commonly with a better development for nanoparticle functionalization. In this approach, other functional materials are coated on the surface of the as-synthesized nanoparticles by chemical or physical interactions such as covalent bond, hydrogen bond, or electrostatic, hydrophilic/hydrophobic, affinity interactions. Philipse et al. [76] reported coating of magnetite nanoparticles by amorphous silica through a sol-gel approach. The silica-coated magnetite nanoparticles are well dispersed in aqueous suspensions. The reverse microemulsion method has been developed for silica coating using non-ionic surfactants such as Triton X100, Brij-97 and Igepal CO-520, giving a uniform silica coating of 1 nm encapsulating the bare nanoparticles [77]. The resulting silica-coated magnetic nanoparticles could be further either functionalized or modified with polymers, yielding multifunctional hybrid nanomaterials [78-82]. Gold has been another inorganic coating candidate to implement functionality to magnetic nanoparticles. The $Au\text{-}Fe_3O_4$ nanoparticles are synthesized by the growth of Au on the surface of Fe_3O_4 nanoparticles through seed-mediated process [83-85]. Gold coating of magnetic nanoparticles provides gold surface which could be easily functionalized with various ligands such as protein, oligonucleotide, DNA sequences though Au-S covalent bonding as reviewed [86].

Various synthetic polymers such as poloxamers, poly(ethyleneglycol) (PEG), and their copolymers or natural polymers such as dextran, chitosan, and gelatin have been widely employed as coatings for stabilization or functionalization purposes. The adsorption of block-copolymers such as poloxamers and poloxamines has been widely studied. Such copolymers adsorb onto the surface of hydro-

phobic Fe_3O_4 nanoparticles via their hydrophobic poly(propylene oxide) (PPO) component, extending the hydrophilic poly(ethylene oxide) (PEO) side-arms outward from the particle surface. The strength of polymer adsorption and the resultant polymer conformation strongly depends on the proportion and the size of both PPO and PEO blocks as well as the physico-chemical properties and the curvature of the Fe_3O_4 nanoparticles [87-89]. A heterobifunctional PEG such as carboxyl-terminated PEG could covalently attach to the Fe_3O_4 nanoparticles surface through carboxyl groups by one end and be further functionalized with other specific molecules such as targeting ligands, drugs or imaging reporter molecules by other end [90-92]. Dextran-coated iron oxide nanoparticles and crosslinked iron oxide nanoparticles have been developed for magnetic resonance imaging applications [93,94]. The crosslinked iron oxide nanoparticles were also treated with ammonia to provide primary amino groups for the attachment of other biomolecules [95,96]. Chitosan-coated Fe_3O_4 nanoparticles have been produced by physical adsorption of chitosan onto oleic acid-coated nanoparticles. Because of having both amino and hydroxyl functional groups, chitosan and its derivatives could form polymeric nanoparticles with nucleic acids and various pharmaceutical formulations through electrostatic interactions [97-99].

Design of Fe_3O_4 nanoparticles for biomedical applications requires careful considerations to the physicochemical stability, targeting ability, drug loading and release. Fig. 7 describes the general design of magnetic nanoparticles for biomedical treatments [100]. The functionalized Fe_3O_4 nanoparticles could carry other active targeting moieties, drugs and imaging agents by both physical interactions and covalent linkages. For example, doxorubicin is loaded on dextran cross-linked iron oxide nanoparticles based on the electrostatic interaction between the positively charged doxorubicin and the negatively charged polymer layer on the surface of nanoparticles [101] while methotrexate (MTX) drug is chemically conjugated to the surface of iron oxide nanoparticles via amide bond [102]. At the targeted location, different release mechanisms could be activated depending on the choice of therapeutic technique integrated onto the magnetic nanoparticles. Respectively, the doxorubicin could be released in the acidic condition of tumor due to the pH change of the surrounding medium, while the MTX drug could be released through an enzymatic reaction by the presence of lysozymes in the lysosomal compartments. The functionalized Fe_3O_4 nanoparticles could be also modified with different dye molecules, resulting in both magnetic and optical detection ability in a single particle. Various types of dye molecules have been attached at the nanoparticle surface for emission in both visible range for in vitro imaging and near infrared region for *in vivo* observation [103-105]. Peptides, antibodies, proteins, and oligonucleotides could be covalently attached on the surface of functionalized Fe_3O_4 nanoparticles. For example, they could be bound to the amino group of a cross-linked dextran iron oxide using different heterofunctional linkers, such as disulfide bound formation, carbon-thiol formation, amide formation, and ether formation [106-109].

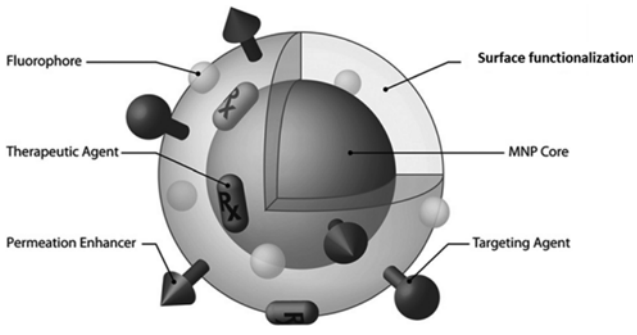

Fig. 7. General design of the magnetic nanoparticles for biomedical treatments [100].

CONTROLLED DRUG DELIVERY APPLICATIONS OF Fe_3O_4 NANOPARTICLES

Controlled drug delivery by nanostructured functional materials is attracting considerable attention because of the high opportunities in cancer treatment. A controlled drug delivery system should be able to deliver drugs to a targeted location in the body, and to maintain drug levels within the required concentration range for therapy. Tumor targeting with magnetic nanoparticles may generally use passive or active strategies. The passive targeting, also called enhanced permeability and retention (EPR) effect, is caused by the production of new blood vessels (the neovasculature) with poor organization and leaky vasculature as a result of fast growth of tumors. The leaky vasculature enables extravasation of nanoparticles into the tumor tissue [110,111]. The active targeting requires specific functionalization of nanoparticle surface with a ligand having high specificity towards cancer cells. Various proteins, peptides, antigenes, antibodies, cytokines, hormones, vitamins, folate, and transferrin are grafted onto the iron oxide nanoparticle surface and *in vitro* studies performed with these functionalized nanoparticles have demonstrated their enhanced cellular uptakes compared to nonfunctionalized nanoparticles [112-118]. In addition, high-gradient of external magnetic fields could be used to guide and concentrate the magnetic nanocarriers at the tumor site [119-121]. The ability to target a specific site reduces the systemic distribution of cytotoxic compounds, and enhances uptake at the target site, resulting in more effective treatment at lower doses. To retain the magnetic particles at the target site, the applied magnetic field must exceed the linear blood flow rates in the vessels which were reported as 10 cm s^{-1} in arteries and 0.05 cm s^{-1} in capillaries [122].

Once the magnetic carrier is concentrated at the target, the therapeutic agent is then released from the magnetic carrier, leading to increased uptake of the drug by the tumor cells at the target sites. The loaded drug could be released by changes in the local physicochemical environment. For example, drug molecule is loaded into the Fe_3O_4 porous/hollow nanoparticles and its release is studied as a function of the pH with a higher release rate in acidic conditions [123]. It is supposed that the acidic environment could weaken the binding between drug molecule and polymer layer on the surface of Fe_3O_4 porous/hollow nanoparticles [124]. One unit decrease in the pH of media causes a pronounced increase in polymer degradation as well as drug release [125]. A higher release in acidic conditions is also attributed to the enlargement of the pores of porous/hollow nanoparticles due to the acid etching of Fe_3O_4 shell [126]. Since the pH of release medium plays a critical role in the drug release from the polymeric coating layer, a small change in biological pH that occurs by disease would result in polymer degradation enough for drug release from the nanocarriers.

Magnetic nanoparticles embedded in a hydrogel which could be mechanically deformed upon application of a static magnetic field or generate heat under an alternating current field were used to deliver drug and control drug release. Chen's group fabricated ferrogels by using an *in-situ* synthesis of magnetic nanoparticles in the presence of various polymers such as poly(vinyl alcohol) and gelatin for controlled drug release [127,128]. The ferrogels consist of an interconnected nanopore structure which could serve as a reservoir to accommodate therapeutic drugs and the nanoporous networks, which are sensitive to the application of a magnetic field. Upon applying a static magnetic field, the particles in the hydrogels aggregate together instantly and produce a bulk magnetic moment, leading to a rapid reduction in the porosity of hydrogel. In this condition, the hydrogel is characterized as a "close" configuration and results in a slower drug release than that when the static magnetic field is off. After the field is removed, the ferrogels return to their original forms. Fig. 8 shows a typical example for the pore size distribution of ferrogels treated with and without magnetic field, the drug release profiles with and without applying magnetic field and the schematic illustration of drug release from the magnetic-sensitive ferrogels with and without applying external magnetic field. This magnetic-induced mechanical deformation of the polymer could be utilized to sustain drug levels within the desired therapeutic range for a long time.

On the contrary with the static magnetic field, drug release from ferrogels is enhanced under an alternating magnetic field [129,130]. The thermal energy from magnetic nanoparticles could be used as an external and remotely controlled trigger for controlled drug release through two distinct types of mechanisms [6]. In the first type, if a drug molecule is attached to magnetic nanoparticles through a linker under application of an alternative magnetic field, the linker is heated and then is detached from the nanoparticle surface, resulting in releasing of the drug molecule. In another manner, if both drug molecules and magnetic nanoparticles are encapsulated within a polymeric matrix, by applying a magnetic field, local heat generated by the magnetic nanoparticles results in formation of crevices or cracks of nanometer scale within a polymeric matrix, thereby encapsulated drugs are released.

The magnetic nanoparticles conjugated with thermoresponsive polymers offered a class of "smart" nanocarriers that have the ability to respond to a change in temperature, which makes them useful materials in a wide range of applications [131]. The poly(ethyleneoxide)-poly(propylene-oxide)-poly(ethylene-oxide) (PEO-PPO-PEO) block copolymers are used to squeeze out hydrophilic drugs

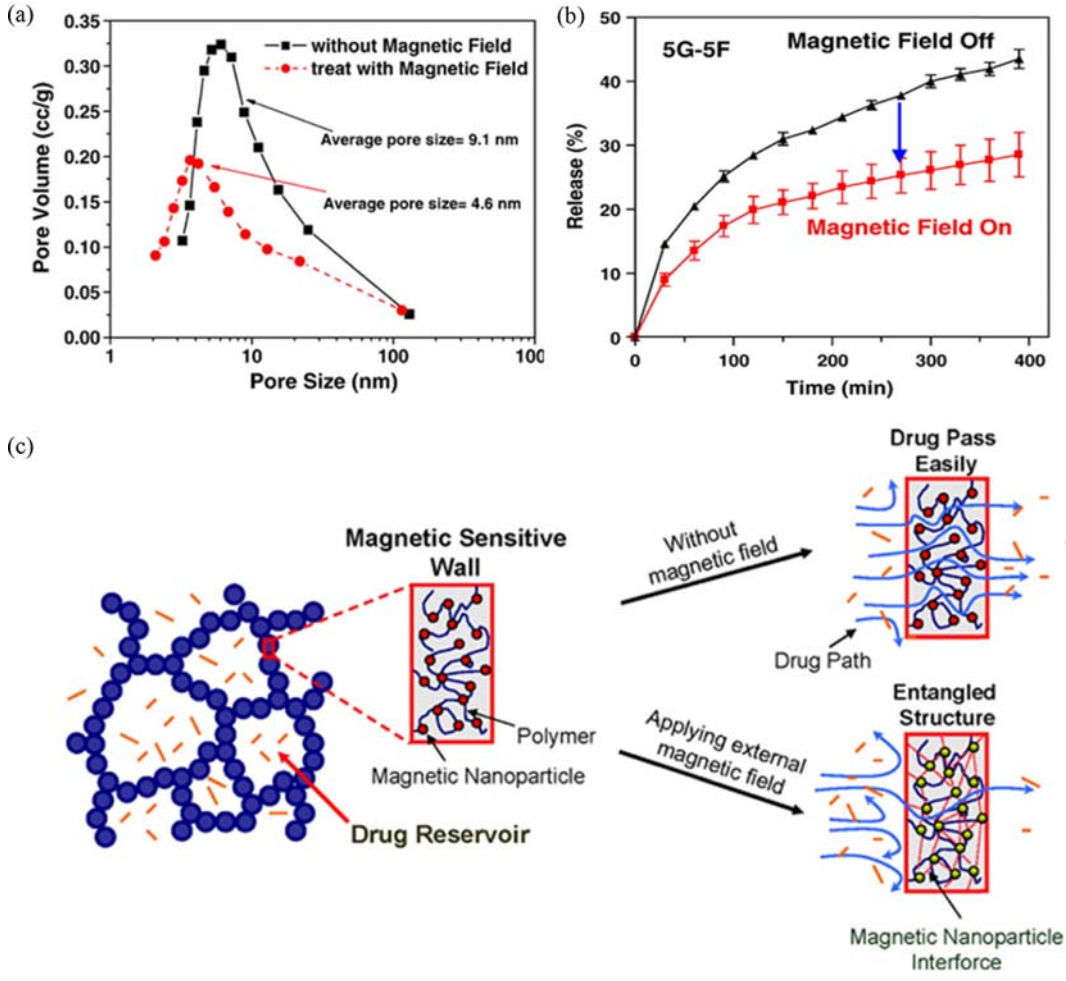

Fig. 8. (a) A typical example for the pore size distribution of the ferrogels treated with and without magnetic field. (b) The drug release profiles with and without applying magnetic field. (c) The schematic illustration of drug release from the magnetic-sensitive ferrogels with and without applying external magnetic field [128].

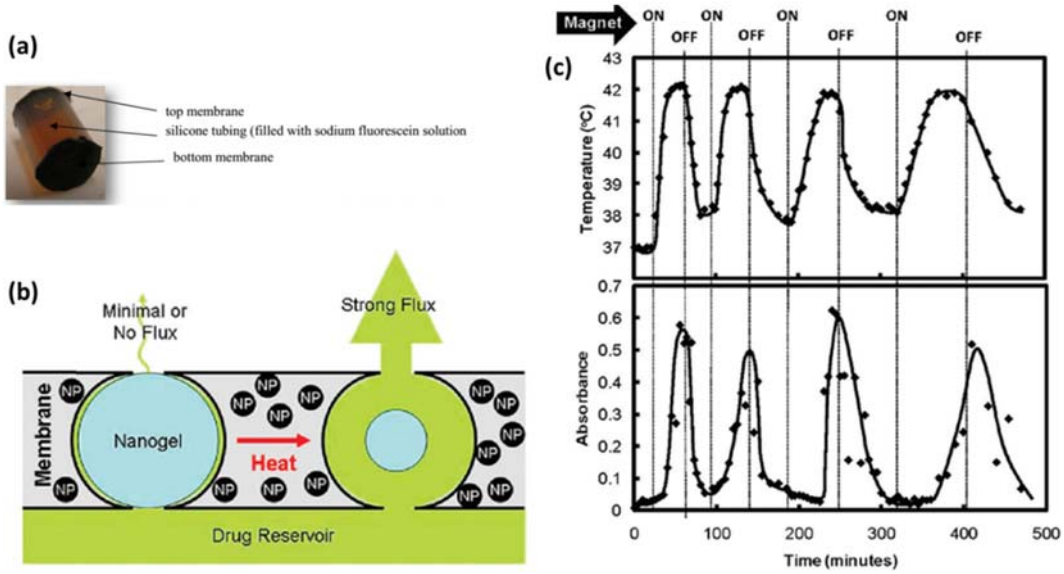

Fig. 9. (a) Picture of membrane capped capsules used for magnetic flux testing. (b) The concept of the "on-demand" drug delivery upon the application of an oscillating magnetic field. (c) Temperature profile in the sample chamber and differential flux of sodium fluorescein out of membrane-capped devices as a function of time over four successive on/off cycles of the external magnetic field [133].

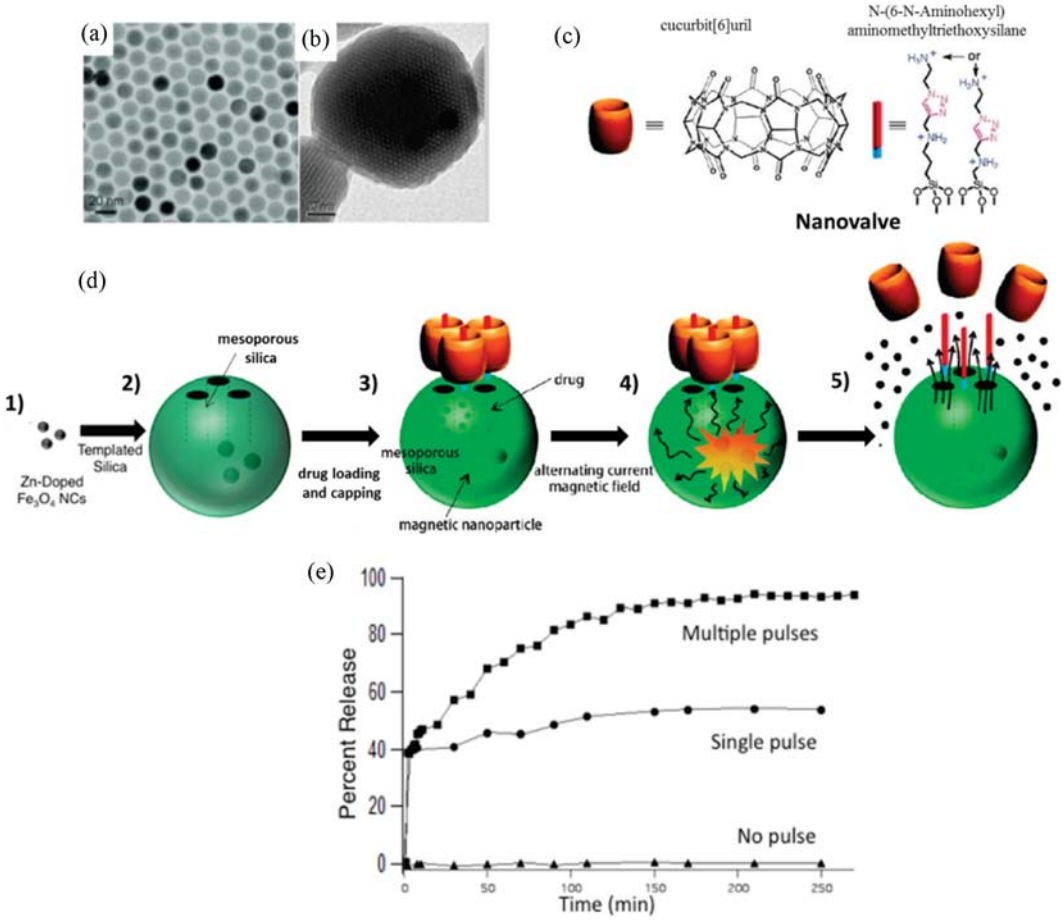

Fig. 10. (a) TEM image of $(Zn_{0.4}Fe_{0.6})Fe_2O_4$ nanoparticles. (b) TEM image of $(Zn_{0.4}Fe_{0.6})Fe_2O_4$ encapsulated silica nanoparticles. (c) Chemical structure of nanovalve. (d) Schematic of nanoparticles formation (1), ecapsulation (2), drug loading and nanovalve assembly (3), pore opening by the local internal heating (4), and drug release (5). (e) Drug release profile monitored during the AC field application with multiple AC field pulses, single initial pulse, and no pulse. The sample was kept at 0 ºC to determine whether internal heating alone causes the valve opening [134].

with magnetic nanoparticles and were investigated for drug release at different temperatures. The profiles of drug release rate were very favorable: very slow at 4 °C and 25 °C, modest at 37 °C, much faster at 45 °C and bursting upon magnetic heating. It has been revealed that, under magnetic heating, burst-like release is observed due to the irreversible and disruptive changes of the magnetic nanoparticle core [132].

Hoare et al. [133] developed nanocomposite membranes based on thermosensitive, poly(N-isopropylacrylamide)-based nanogels and magnetite nanoparticles entrapped in ethyl cellulose to achieve "on-demand" drug delivery upon the application of an oscillating magnetic field as shown in Fig. 9. Magnetic triggering is evaluated in small-scale devices made by gluing two 1 cm diameter membrane disks to the ends of a 1 cm length of silicone tubing filled with a sodium fluorescein solution (Fig. 9(a)). The devices are mounted inside a flow cell placed in a solenoid coil. A constant water flow is maintained through the cell to permit continuous sampling of fluorescein release. Under an oscillating applied field, heat generated by magnetite nanoparticles is transferred to the adjacent thermosensitive nanogels, causing the nanogels to shrink and permit drug diffusion out of the device. When the magnetic field is turned off, the nanogels reswell and refill the membrane pores, resulting in the return to a near-zero value of drug flux. A 10- to 20-fold differential flux is observed between the "on" and "off" states as shown in Fig. 9(c).

The thermal energy from magnetic heating was utilized to open the gates of inorganic carriers which contain drugs for therapy as shown in Fig. 10. Thomas et al. [134] synthesized 15 nm $(Zn_{0.4}Fe_{0.6})Fe_2O_4$ nanoparticles and then incorporated these nanoparticles inside porous drug carrier nanoparticles. Nanovalves, which consisted of N-(6-N-Aminohexyl) aminomethyltriethoxysilane and cucurbit[6]uril, were capped onto the pores to keep the drug inside. When an external alternating magnetic field was applied, heat generation and a subsequent pressure buildup inside the porous nanoparticles caused the rapid removal of molecular valves and the rapid release of drug molecules. These magnetic nanoparticles are considered as effective actuators for controlled drug release from a carrier. When breast cancer cells (MDA-MB-231) were treated with doxorubicin-loaded particles and exposed to an alternating magnetic field, cell death occurred. This material promises to be a noninvasive, externally controlled drug delivery system with cancer-killing properties.

The heat generation from magnetic nanoparticles was used to remotely activate temperature-sensitive cation channels within cells without observable toxic effects as shown in Fig. 11 [135]. In this study, superparamagnetic $MnFe_2O_4$ nanoparticles were targeted to specific proteins on the plasma membrane of cells exposing the transient receptor potential cation channel subfamily V member 1 (TRPV1), and then were heated by a radio-frequency magnetic field. On the application of oscillating magnetic field, the local temperature increased, resulting in heat-induced opening of TRPV1 and caused an influx of calcium ions into the cells. This approach could be applied to activate cells uniformly across a large volume, making it feasible for *in vivo* whole-body applications.

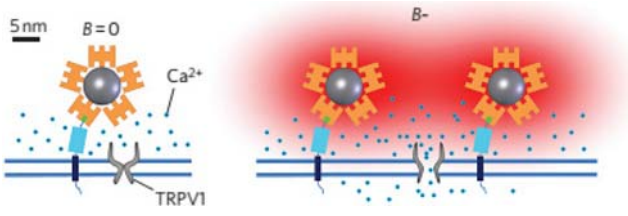

Fig. 11. Schematic showing local heating of streptavidin–DyLight549 (orange)-coated superparamagnetic nanoparticles (grey) in a RF magnetic field (B~) and heat (red)-induced opening of TRPV1 [135].

MAGNETIC HYPERTHERMIA APPLICATIONS OF Fe_3O_4 NANOPARTICLES

The use of magnetic nanoparticles for hyperthermia has shown great promise in the field of disease treatment. By applying an alternative magnetic field with sufficient amplitude and frequency, the magnetization of the particles is continuously reversed, which converts magnetic into thermal energy. This heat is immediately released to the surrounding tumor cells. By raising the temperature of tissues to between 42 °C and 46 °C, the viability of the disease tissues is reduced and their sensitivity to chemotherapy and radiation is increased [136-139]. In addition to selectively killing tumor cells, a potential of developing antitumor immunity after hyperthermia treatment has been also suggested [140-142].

The actual increase in temperature at a targeted site due to the conversion of magnetic energy loss not only depends on the intrinsic magnetic properties of materials and the applied field, but also on the local blood circulation and the thermal conductivity and heat capacity of surrounding medium. It should be considered that the impact of the alternative magnetic field on human body is connected with heating effects due to eddy currents induced in the electrically conducting tissue. Several studies reported that a magnetic field of 150 kHz frequency and 80 kA m^{-1} amplitude seriously affected an animal body [143,144]. It has been suggested that the upper limit for the magnetic field (product of the amplitude, H, and frequency, f) should not exceed 4.85×10^8 A/m s^{-1} [145], or 5×10^9 A/m s^{-1} [146].

General mechanisms for heat generation of different magnetic nanoparticles are given in Fig. 12. For superparamagnetic nanoparticles, the external magnetic field supplies energy and assists the magnetic moment rotation inside particles. This energy is dissipated with the relaxation of the magnetic moment to its equilibrium orientation, or so-called Néel relaxation. The Néel relaxation mechanism is characterized by the time constant to return to equilibrium of the magnetization after a perturbation. It depends on the magnetic anisotropy energy barrier which needs to overcome for the reversal of magnetization. Certainly, the magnetic anisotropy energy barrier depends on two main parameters: the intrinsic anisotropy of particle (material, surface and shape) and the volume of particle.

A so-called hysteresis loss mechanism dominates heat generation of ferromagnetic materials whose sizes exceed the domain wall width. Under application of an alternative field, the magnetic moments oscillate and cause domain wall displacement, which generates heat. The heat generation depends not only on the applied field but also on the magnetic pre-history of material, which is governed by the intrinsic factors of material such as particle structure (size, shape and crystal structure), magnetic properties (magnetic anisotropy and temperature dependence of magnetizations). When the applied field is small, the hysteresis loops differ from full hysteresis loops in that they are minor loops having relatively smaller areas, and the

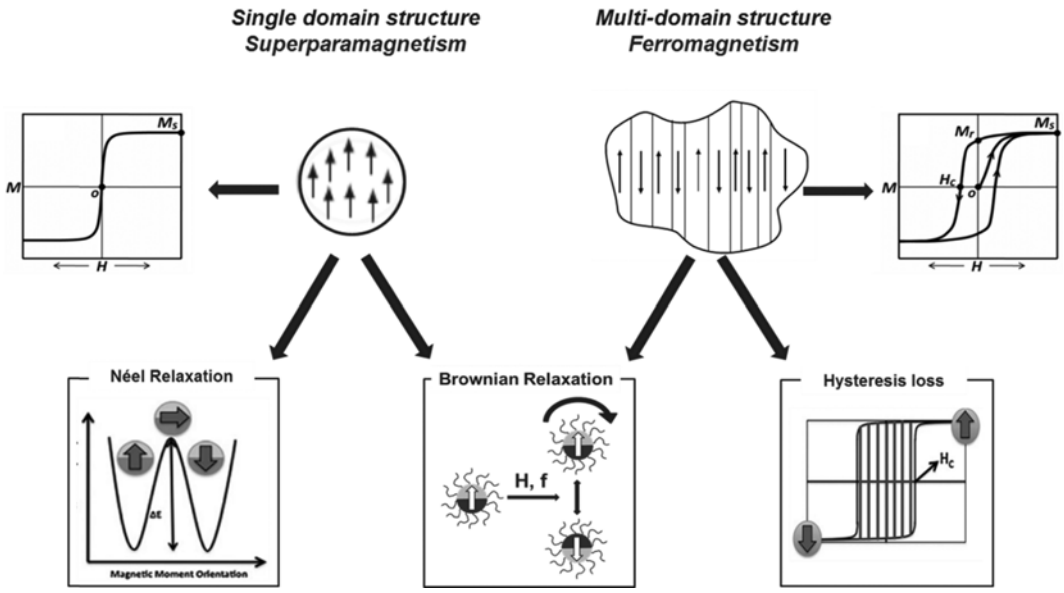

Fig. 12. General mechanisms for heat generation of magnetic nanoparticles.

amount of heat generated is considered to be proportional to the frequency multiplied by the area of the loop [147,148].

Heat generation is also caused by the rotational Brownian motion within a dispersed medium because of the torque exerted on the magnetic moment by the external alternating magnetic field. In this case, the thermal energy is delivered through shear stress in the surrounding fluid. The rotation ability is characterized by the viscosity of medium and the global hydrodynamic diameter of particle. In practice, due to the high viscosity of the intracellular medium, the Brownian relaxation mechanisms could be significantly hindered, and consequently the performance of the nanoparticles mainly depends on their above primitive mechanisms [149-151].

The Brownian relaxation and other primitive heating mechanisms take place in parallel but with different contributions to overall heat generation. The contribution of Brownian relaxation to heating was experimentally investigated by using a molten and solidified gel to prevent free rotation of the particle. A comparative study between superparamagnetic (8 nm in diameter) and ferromagnetic (up to several hundred nanometers in diameter) magnetite particles suspended in a commercial gel which could be melted above 30 °C was reported as shown in Fig. 13 [152]. The heating rate of the gel containing superparamagnetic nanoparticles showed no difference between below (Néel relaxation only) and above (Néel and Brownian relaxations) the melting point with the heating rate of about 3.5 °C min^{-1}, while for ferromagnetic nanoparticles, a big difference of loss power was found before the gel melting (hysteresis losses only) with the heating rate of 1 °C min^{-1} and after the melting point (hysteresis losses and Brown relaxation) with the heating rate of 15 °C min^{-1}. This revealed that, for superparamagnetic particles, the Brownian relaxation exhibited an insignificant contribution to overall heat generation in comparison with Néel relaxation and, for ferromagnetic particles, a proper coating would greatly influence heating via Brownian mechanism.

Magnetic particles which have been studied for use in hyperthermia treatment have been focused on the magnetite Fe_3O_4 and the nanoparticles related with cobalt, nickel, or other substitutions in

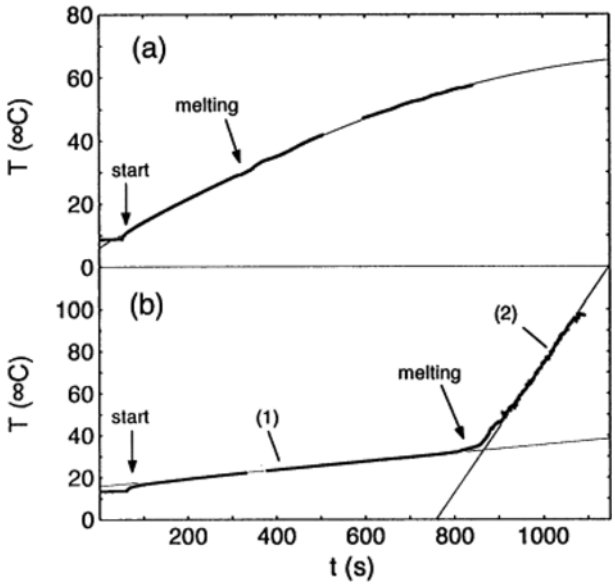

Fig. 13. Temperature increase due to the heating of magnetite particles in Rf-field (410 kHz, 6.5 kA m^{-1}) for (a) superparamagnetite nanoparticles of 8 nm and (b) ferromagnetic particles of several hundred nanometers suspended in commercial gel [152].

size from several nanometers to a few tenths of a micron. The main parameter to determine the heating of tissue is the specific loss power (SLP) or specific absorption rate (SAR), which can be calculated based on the following equation:

$$SLP(SAR) = \frac{c}{m}\frac{\Delta T}{\Delta t}$$

where C represents the sample specific heat capacity, m is the amount of magnetic material per mass or volume of sample used in the experiment and ($\Delta T/\Delta t$) is the initial slope of heating curve.

The higher the specific loss power is, the lower the injected dose

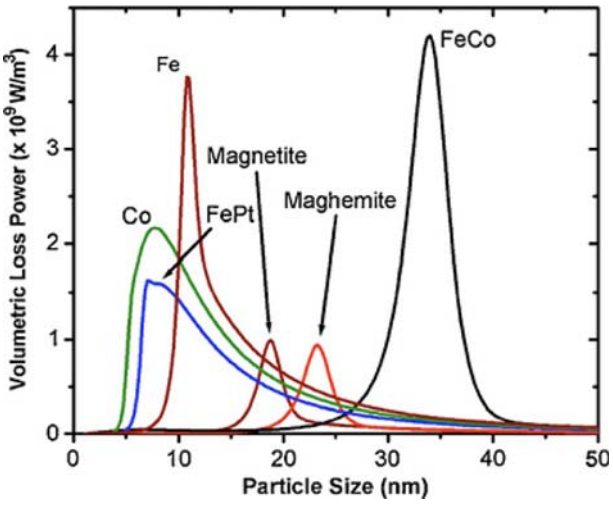

Fig. 14. Theoretical size-dependent volumetric SLP values for different magnetic nanoparticles in single domain regime [156].

to the patient can be. The hyperthermia efficiency which could be reflected by heating rate or SLP values depends on various factors, including the intrinsic factors of material such as particle structure, magnetic properties and the external factors such as amplitude and frequency of the applied magnetic field [153-155]. Rosensweig [53] formulated and computed heating rates for various magnetic samples and reported that the highest heating rates could be provided by magnetite among several different materials. The heating rate of a given particle size depends on the applied field intensity but the optimum particle size which could yield maximum heating rate is nearly independent of the applied field intensity. A very sharp maximum of the heating rate was observed for monodisperse Fe_3O_4 nanoparticles of about 14 nm diameter. Rosensweig's calculation also revealed that an increase of the size distribution caused a very fast decrease of the heating rate. By using available data for domain magnetization and magnetic anisotropy constant, the dependence of SLP values on particle size was predicted for various materials in single domain regime as shown in Fig. 14 [156].

Practically, the effect of each significant parameter such as particle size and shape, functionalization, magnetic properties on the hyperthermia efficiency has been independently investigated from study to study with different particle synthesis methods and different magnetic-induced heating systems. Ma et al. [157] reported that the SLP values depended on the particle size and the coercivity of Fe_3O_4 nanoparticles. Under an applied field of 80 kHz frequency and 32.5 kA m^{-1} amplitude, a maximum SLP was recorded for sample containing 46 nm diameter of Fe_3O_4 nanoparticles which also has the highest coercivity. Gonzales-Weimuller et al. [158] demonstrated that SLP values of superparamagnetic Fe_3O_4 nanoparticles varied with particle size. The highest SLP was measured for 11.2 nm particles under an applied field of 400 kHz frequency and 24.5 kA m^{-1} amplitude and their models indicated that higher heating rates are possible by increasing the size of particles to 12.5 nm. Gonzalez-Fernandez et al. [159] used an alternative magnetic field of 260 kHz frequency and 100 Oe (about 8 kA m^{-1}) amplitude to induce heat generation and showed a strong dependence of the SLP on the size of Fe_3O_4 nanoparticles with a maximum of SLP for particles of around 30 nm diameter. It should also be noticed that an evolution of aggregation of the nanoparticles caused a modification of the SLP values due to the effect of dipolar interparticle coupling with Néel relaxation. With a proper coating, a ferromagnetic nanoparticle could give a fast heating rate for disease treatment. For instance, chitosan oligosaccharide-stabilized iron oxide nanocubes (Chito-FIONs) were developed for cancer hyperthermia [160]. The Chito-FIONs encapsulated with multiple 30-nm-sized iron oxide nanocubes showed higher hyperthermal efficiency than single nanocube. Compared with commercial Feridex nanoparticles, the SLP of the Chito-FIONs was more than 30 times higher than that of the Feridex.

Temperature control during heating is essential, but still remains challenging because heat conduction and energy adsorption *in vivo* are widely unknown and local overheating may damage the healthy tissue. Achieving self-controlled and self-regulated heating by developing materials with the Curie temperature slightly above the therapeutic temperature (approx. 45 °C) has been considered as an effective method to prevent such local overheating problem. The Curie temperature (T_C) is the maximal temperature reachable by magnetic particles to maintain their magnetic properties. Above this temperature, magnetic particles lose their magnetic properties, and thus they do not convert electromagnetic energy into heat. Syntheses of several materials such as $La_{1-x}Sr_xMnO_3$, $M_{1-x}Zn_xFe_2O_4$ (with M=Ni, Cu, Co, Mn) and $Ni_{1-x}Cr_x$ alloy with adjustable T_C have been reported [161-164]. Certainly, an ideal material with optimal physical features for self-controlled and self-regulated magnetic heating has not been well developed yet but, indeed, this concept offers a smart way to control hyperthermia.

CONCLUSIONS

The concepts of drug delivery and hyperthermia using magnetic nanoparticles have developed rapidly from the benefit of advanced nanotechnologies, which enable us not only to produce magnetic nanoparticles of a specific shape in a narrow size distribution range but also to engineer particle surfaces to manipulate their characteristics. Different kinds of monodisperse nanoparticles with controllable particle sizes and compositions could be synthesized by various synthetic procedures. Such magnetic nanoparticles tend to form agglomerates to reduce the energy associated with the magnetic property and the high surface area to volume ratio of the nanosized particles. It has been crucial to develop surface coating strategies that should be optimized to simplify the process and to effectively prevent any aggregation and sedimentation of the magnetic nanoparticles to improve their stability as well as to develop and provide a stable injectable solution for biomedical treatments. Surface coating of magnetic nanoparticles also provides new surfaces which can be easily functionalized with various ligands such as protein, oligonucleotide, DNA by both physical interactions and covalent linkages. However, the effects of surface coating on the magnetic property of nanoparticles should be carefully considered.

Controlled drug delivery and hyperthermia treatment by magnetic nanoparticles exhibits high opportunities in biomedical treatments. High-gradient, external magnetic fields could be utilized to guide and concentrate the magnetic nanocarriers at tumor locations. Once the magnetic carrier is concentrated at the target, the therapeutic agent is released from the magnetic carrier by changes in the

local physicochemical environment or by application of an external magnetic field, leading to the increased uptake of drug by the tumor cells. By applying an alternative magnetic field with sufficient amplitude and frequency, the magnetization of the particles is continuously reversed, which converts magnetic to thermal energy. A combination of hyperthermia-based therapy and controlled drug release has strong potential to develop an intelligent therapy for cancer treatment. However, it is still a great challenge to develop a system that minimizes nanoparticle dose for actual treatment. This could be overcome by synthesis and surface modification of nanoparticles able to circulate in the blood compartment for a long period and bearing ligands able to facilitate their specific internalization in tumor cells. Finally, the biomedical uses of magnetic nanoparticles are not restricted to controlled drug delivery and hyperthermia; indeed, they are also applicable to magnetic resonance imaging, bioseparation, sensing, enzyme immobilization, immunoassays, and so on.

ACKNOWLEDGEMENTS

This work was supported by the Regional Innovation Center for Environmental Technology of Thermal Plasma (ETTP) at Inha University, designated by MKE (2009). This study was also supported by 2013 Research Grant from Kangwon National University (No. 120131220).

REFERENCES

1. C. Yang, J. Wu and Y. Hou, *Chem. Commun.*, **47**, 5130 (2011).
2. A.-H. Lu, E.L. Salabas and F. Schuth, *Angew. Chem. Int. Ed.*, **46**, 1222 (2007).
3. S. Laurent, D. Forge, M. Port, A. Roch, C. Robic, L. V. Elst and R. N. Muller, *Chem. Rev.*, **108**, 2064 (2008).
4. N. Lee and T. Hyeon, *Chem. Soc. Rev.*, **41**, 2575 (2012).
5. C. Sun, J. S. H. Lee and M. Zhang, *Adv. Drug Deliv. Rev.*, **60**, 1252 (2008).
6. C. S. S. R. Kumar and F. Mohammad, *Adv. Drug Deliv. Rev.*, **63**, 789 (2011).
7. R. Massart, *IEEE Trans. Magn.*, **17**, 1247 (1981).
8. L. Vayssières, C. Chanéac and E. Tronc, *J. Colloid Interface Sci.*, **205**, 205 (1998).
9. G. Gnanaprakash, S. Mahadevan, T. Jayakumar, P. Kalyanasundaram, J. Philip and B. Raj, *Mater. Chem. Phys.*, **103**, 168 (2007).
10. J. P. Jolivet, P. Belleville, E. Tronc and J. Livage, *Clays Clay Miner.*, **40**, 531 (1992).
11. J. P. Jolivet, C. Chaneac and E. Tronc, *Chem. Commun.*, **5**, 481 (2004).
12. S. Sun and H. Zeng, *J. Am. Chem. Soc.*, **124**, 8204 (2002).
13. S. Sun, H. Zeng, D. B. Robinson, S. Raoux, P. M. Rice, S. X. Wang and G. Li, *J. Am. Chem. Soc.*, **126**, 273 (2004).
14. Z. C. Xu, C. M. Shen, Y. L. Hou, H. J. Gao and S. S. Sun, *Chem. Mater.*, **21**, 1778 (2009).
15. N. R. Jana, Y. F. Chen and X. G. Peng, *Chem. Mater.*, **16**, 3931 (2004).
16. W. Cai and J. Wan, *J. Colloid Interface Sci.*, **305**, 366 (2007).
17. T. Hyeon, S. S. Lee, J. Park, Y. Chung and H. B. Na, *J. Am. Chem. Soc.*, **123**, 12798 (2001).
18. J. Park, E. Lee, N. M. Hwang, M. Kang, S. C. Kim, Y. Hwang, J. G. Park, H. J. Noh, J. Y. Kim, J. H. Park and T. Hyeon, *Angew. Chem. Int. Ed.*, **44**, 2872 (2005).
19. J. Park, K. An, Y. Hwang, J. G. Park, H. J. Noh, J. Y. Kim, J. H. Park, N. M. Hwang and T. Hyeon, *Nat. Mater.*, **3**, 891 (2004).
20. S. G. Kwon, Y. Piao, J. Park, S. Angappane, Y. Jo, N.-M. Hwang, J.-G. Park and T. Hyeon, *J. Am. Chem. Soc.*, **129**, 12571 (2007).
21. J. Ge, Y. Hu, M. Biasini, W. P. Beyermann and Y. Yin, *Angew. Chem. Int. Ed.*, **46**, 4342 (2007).
22. L. Zhang, R. He and H. C. Gu, *Mater. Res. Bull.*, **41**, 260 (2006).
23. R. Swaminathan, M. A. Willard and M. E. Mchenry, *Acta Mater.*, **54**, 807 (2006).
24. H. P. Qi, Q. W. Chen, M. S. Wang, M. H. Wen and J. Xiong, *J. Phys. Chem. C*, **113**, 17301 (2009).
25. D. Kim, N. Lee, M. Park, B. H. Kim, K. An and T. Hyeon, *J. Am. Chem. Soc.*, **131**, 454 (2009).
26. L. Zhao, H. Zhang, Y. Xing, S. Song, S. Yu, W. Shi, X. Guo, J. Yang, Y. Lei and F. Cao, *Chem. Mater.*, **20**, 198 (2008).
27. X. Li, Z. Si, Y. Lei, J. Tang, S. Wang, S. Su, S. Song, L. Zhao and H. Zhang, *Cryst. Eng. Comm.*, **12**, 2060 (2010).
28. X. F. Qu, Q. Z. Yao, G. T. Zhou, S. Q. Fu and J. L. Huang, *J. Phys. Chem. C*, **114**, 8734 (2010).
29. S. Palchoudhury, Y. Xu, J. Goodwin and Y. Bao, *J. Appl. Phys.*, **109**, 07E314 (2011).
30. F. Caruso, M. Spasova, A. Susha, M. Giersig and R. A. Caruso, *Chem. Mater.*, **13**, 109 (2001).
31. Z. Huang and F. Tang, *J. Colloid Interface Sci.*, **281**, 432 (2005).
32. S. Peng and S. Sun, *Angew. Chem. Int. Ed.*, **46**, 4155 (2007).
33. J. Huang, W. Chen, W. Zhao, Y. Li, X. Li and C. Chen, *J. Phys. Chem. C*, **113**, 12067 (2009).
34. H. J. Fan, U. Gçsele and M. Zacharias, *Small*, **3**, 1660 (2007).
35. C. M. Wang, D. R. Baer, L. E. Thomas, J. E. Amonette, J. Antony, Y. Qiang and G. Duscher, *J. Appl. Phys.*, **98**, 094308 (2005).
36. R. Nakamura, D. Tokozakura, H. Nakajima, J. G. Lee and H. Mori, *J. Appl. Phys.*, **101**, 074303 (2007).
37. R. Nakamura, J. G. Lee, D. Tokozakura, H. Mori and H. Nakajima, *Mater. Lett.*, **61**, 1060 (2007).
38. Y. Piao, J. Kim, H. B. Na, D. Kim, J. S. Baek, M. K. Ko, J. H. Lee, M. Shokouhimehr and T. Hyeon, *Nat. Mater.*, **7**, 242 (2008).
39. H. Wu, S. Zhang, J. Zhang, G. Liu, J. Shi, L. Zhang, X. Cui, M. Ruan, Q. He and W. Bu, *Adv. Funct. Mater.*, **21**, 1850 (2011).
40. L. P. Zhu, H. M. Xiao, W. D. Zhang, G. Yang and S. Y. Fu, *Cryst. Growth Des.*, **8**, 957 (2008).
41. S. Liu, R. Xing, F. Lu, R. K. Rana and J. J. Zhu, *J. Phys. Chem. C*, **113**, 21042 (2009).
42. P. Hu, L. Yu, A. Zuo, C. Guo and F. Yuan, *J. Phys. Chem. C*, **113**, 900 (2009).
43. C. Cheng, F. Xu and H. Gu, *New J. Chem*., **35**, 1072 (2011).
44. X. Chen, Z. Zhang, X. Li and C. Shi, *Chem. Phys. Lett.*, **422**, 294 (2006).
45. X. Lin, G. Ji, Y. Liu, Q. Huang, Z. Yang and Y. Du, *Cryst. Eng. Comm.*, **14**, 8658 (2012).
46. D. T. Nguyen and K.-S. Kim, *AIChE J.*, **59**, 3594 (2013).
47. D. T. Nguyen and K.-S. Kim, *J. Nanosci. Nanotechnol.*, **13**, 5773 (2013).
48. D. T. Nguyen, D.-W. Park, T. Kim and K.-S. Kim, *J. Nanosci. Nanotechnol.*, In Press.
49. J. M. D. Coey, *Magnetism and magnetic materials*, Cambridge Uni-

versity Press (2009).
50. D. L. Leslie-Pelecky, *Chem. Mater.*, **8**, 1770 (1996).
51. C. P. Bean and J. D. Livingston, *J. Appl. Phys.*, **30**, 120S (1959).
52. K. M. Krishnan, *IEEE Trans. Magn.*, **46**, 2523 (2010).
53. R. E. Rosensweig, *J. Magn. Magn. Mater.*, **252**, 370 (2002).
54. D. Yoo, J.-H. Lee, T.-H. Shin and J. Cheon, *Acc. Chem. Res.*, **44**, 863 (2011).
55. D. T. Margulies, F. T. Parker, F. E. Spada, R. S. Goldman, J. Li, R. Sinclair and A. E. Berkowitz, *Phys. Rev. B*, **53**, 9175 (1996).
56. R. H. Kodama, *J. Magn. Magn. Mater.*, **200**, 359 (1999).
57. Y. Yuan, D. Rende, C. L. Altan, S. Bucak, R. Ozisik and D.-A. Borca-Tasciuc, *Langmuir*, **28**, 13051 (2012).
58. L. E. W. LaConte, N. Nitin, O. Zurkiya, D. Caruntu, C. J. O'Connor, X. P. Hu and G. Bao, *J. Magn. Reson. Imaging*, **26**, 1634 (2007).
59. H. Duan, M. Kuang, X. Wang, Y. A. Wang, H. Mao and S. Nie, *J. Phys. Chem. C*, **112**, 8127 (2008).
60. J. F. Hochepied and M. P. Pileni, *J. Appl. Phys.*, **87**, 2472 (2000).
61. J. F. Hochepied, P. Bonville and M. P. Pileni, *J. Phys. Chem. B*, **104**, 905 (2000).
62. Z. Beji, A. Hanini, L. S. Smiri, J. Gavard, K. Kacem, F. Villain, J.-M. Greneche, F. Chau and S. Ammar, *Chem. Mater.*, **22**, 5420 (2010).
63. J.-T. Jang, H. Nah, J.-H. Lee, S. H. Moon, M. G. Kim and J. Cheon, *Angew. Chem. Int. Ed.*, **48**, 1234 (2009).
64. J. Nogus, J. Sort, V. Langlais, V. Skumryev, S. Surinach, J. S. Munoz and M. D. Baro, *Phys. Rep.*, **422**, 65 (2005).
65. T.-J. Yoon, H. Lee, H. Shao and R. Weissleder, *Angew. Chem. Int. Ed.*, **50**, 4663 (2011).
66. L.-M. Lacroix, N. F. Huls, D. Ho, X. Sun, K. Cheng and S. Sun, *Nano Lett.*, **11**, 1641 (2011).
67. A. K. Gupta and M. Gupta, *Biomaterials*, **26**, 3995 (2005).
68. J. K. Oh and J. M. Park, *Prog. Polym. Sci.*, **36**, 168 (2011).
69. M. Mahmoudia, S. Sant, B. Wang, S. Laurent and T. Sen, *Adv. Drug Deliv. Rev.*, **63**, 24 (2011).
70. Z. Li, L. Wei, M. Y. Gao and H. Lei, *Adv. Mater.*, **17**, 1001 (2005).
71. S. Mohapatra, N. Pramanik, S. K. Ghosh and P. Pramanik, *J. Nanosci. Nanotechnol.*, **6**, 823 (2006).
72. R. F. Ziolo, E. P. Giannelis, B. A. Weinstein, M. P. O'Horo, B. N. Ganguly, V. Mehrotra, M. W. Russell and D. R. Huffman, *Science*, **257**, 219 (1992).
73. F. Llanes, D. H. Ryan and R. H. Marchessault, *Int. J. Biol. Macromol.*, **27**, 35 (2000).
74. Y. Nishio, A. Yamada, K. Ezaki, Y. Miyashita, H. Furukawa and K. Horie, *Polymer*, **45**, 7129 (2004).
75. P. V. Finotelli, M. A. Morales, M. H. Rocha-Leao, E. M. B. Saitovitch and A. M. Rossi, *Mater. Sci. Eng.*, **24**, 625 (2004).
76. A. P. Philipse, M. P. B. Vanbruggen and C. Pathmamanoharan, *Langmuir*, **10**, 92 (1994).
77. S. Santra, R. Tapec, N. Theodoropoulou, J. Dobson, A. Hebard and W. Tan, *Langmuir*, **17**, 2900 (2001).
78. N. Kohler, G. E. Fryxell and M. Q. Zhang, *J. Am. Chem. Soc.*, **126**, 7206 (2004).
79. H. Lee, E. Lee, D. K. Kim, N. K. Jang, Y. Y. Jeong and S. Jon, *J. Am. Chem. Soc.*, **128**, 7383 (2006).
80. H. Lee, M. K. Yu, S. Park, S. Moon, J. J. Min, Y. Y. Jeong, H.-W. Kang and S. Jon, *J. Am. Chem. Soc.*, **129**, 12739 (2007).
81. G. Li, D. L. Zeng, L. Wang, B. Zong, K. G. Neoh and E. T. Kang, *Macromolecules*, **42**, 8561 (2009).
82. J. Zhou, L. Meng, Q. Lu, J. Fu and X. Huang, *Chem. Commun.*, 6370 (2009).
83. Z. Xu, Y. Hou and S. Sun, *J. Am. Chem. Soc.*, **129**, 8698 (2007).
84. I. Y. Goon, L. M. H. Lai, M. Lim, P. Munroe, J. J. Gooding and R. Amal, *Chem. Mater.*, **21**, 673 (2009).
85. D. T. Nguyen, D.-W. Park and K.-S. Kim, *J. Nanosci. Nanotechnol.*, **11**, 7214 (2011).
86. D. T. Nguyen, D.-J. Kim and K.-S. Kim, *Micron*, **42**, 207 (2011).
87. S. M. Moghimi, *Biochem. Biophys. Acta*, **1336**, 1 (1997).
88. J. T. Li, K. D. Caldxell and N. Rapoport, *Langmuir*, **10**, 4475 (1994).
89. S. M. Moghimi and A. C. Hunter, *Trends Biotechnol.*, **18**, 412 (2000).
90. O. Veiseh, C. Sun, J. Gunn, N. Kohler, P. Gabikian, D. Lee, N. Bhattarai, R. Ellenbogen, R. Sze, A. Hallahan, J. Olson and M. Q. Zhang, *Nano Lett.*, **5**, 1003 (2005).
91. C. Sun, R. Sze and M. Q. Zhang, *J. Biomed. Mater. Res. A*, **78A**, 550 (2006).
92. J. F. Lutz, S. Stiller, A. Hoth, L. Kaufner, U. Pison and R. Cartier, *Biomacromolecules*, **7**, 3132 (2006).
93. T. Shen, R. Weissleder, M. Papisov, A. Bogdanov Jr. and T. J. Brady, *Magn. Reson. Med.*, **29**, 599 (1993).
94. L. Josephson, C. H. Tung, A. Moore and R. Weissleder, *Bioconjugate Chem.*, **10**, 186 (1999).
95. P. Wunderbaldinger, L. Josephson and R. Weissleder, *Bioconjugate Chem.*, **13**, 264 (2002).
96. E. A. Schellenberger, A. Bogdanov Jr., D. Hogemann, J. Tait, R. Weissleder and L. Josephson, *Mol. Imaging*, **1**, 102 (2002).
97. E. H. Kim, H. S. Lee, B. K. Kwak and B. K. Kim, *J. Magn. Magn. Mater.*, **289**, 328 (2005).
98. E. H. Kim, Y. Ahn and H. S. Lee, *J. Alloys Compd.*, **434**, 633 (2007).
99. S. R. Bhattarai, S. Y. Kim, K. Y. Jang, K. C. Lee, H. K. Yi, D. Y. Lee, H. Y. Kim and P. H. Hwang, *J. Virol. Methods*, **147**, 213 (2008).
100. C. Sun, J. S. H. Lee and M. Zhang, *Adv. Drug Deliv. Rev.*, **60**, 1252 (2008).
101. M. K. Yu, Y. Y. Jeong, J. Park, S. Park, J. W. Kim, J. J. Min, K. Kim and S. Jon, *Angew. Chem. Int. Ed.*, **47**, 5362 (2008).
102. N. Kohler, C. Sun, J. Wang and M. Q. Zhang, *Langmuir*, **21**, 8858 (2005).
103. C.-W. Lu, Y. Hung, J.-K. Hsiao, M. Yao, T.-H. Chung, Y.-S. Lin, S.-H. Wu, S.-C. Hsu, H.-M. Liu, C.-Y. Mou, C.-S. Yang, D.-M. Huang and Y.-C. Chen, *Nano Lett.*, **7**, 149 (2007).
104. J. H. Lee, Y. W. Jun, S. I. Yeon, J. S. Shin and J. Cheon, *Angew. Chem. Int. Ed.*, **45**, 8160 (2006).
105. L. Josephson, M. F. Kircher, U. Mahmood, Y. Tang and R. Weissleder, *Bioconjugate Chem.*, **13**, 554 (2002).
106. L. Josephson, C. H. Tung, A. Moore and R. Weissleder, *Bioconjugate Chem.*, **10**, 186 (1999).
107. D. Hogemann, L. Josephson, R. Weissleder and J. P. Basilion, *Bioconjugate Chem.*, **11**, 941 (2000).
108. H. W. Kang, L. Josephson, A. Petrovsky, R. Weissleder and A. J. Bogdanov, *Bioconjugate Chem.*, **13**, 122 (2002).
109. E. A. Schellenberger, D. E. Sosnovik, R. Weissleder and L. Josephson, *Bioconjugate Chem.*, **15**, 1062 (2004).
110. R. K. Jain, *Annu. Rev. Biomed. Eng.*, **1**, 241 (1999).
111. R. K. Jain, *J. Controlled Release*, **74**, 7 (2001).
112. D. L. J Thorek, A. Chen, J. Czupryna and A. Tsourkas, *Ann. Biomed.*

Eng., **34**, 23 (2006).
113. J. R. McCarthy and R. Weissleder, *Adv. Drug Deliv. Rev.*, **60**, 1241 (2008).
114. C. C. Berry, *J. Phys. D: Appl. Phys.*, **42**, 224003 (2009).
115. J. Corchero and A. Villaverde, *Trends Biotechnol.*, **27**, 468 (2009).
116. U. S. Toti, B. R. Guru, A. E. Grill and J. Panyam, *Mol. Pharm.*, **7**, 1108 (2010).
117. X. Yang, J. J. Grailer, I. J. Rowland, A. Javadi, S. A. Hurley, D. A. Steeber and S. Gong, *Biomaterials*, **31**, 9065 (2010).
118. D. Cheng, G. Hong, W. Wang, R. Yuan, H. Ai, J. Shen, B. Liang, J. Gao and X. Shuai, *J. Mater. Chem.*, **21**, 4796 (2011).
119. B. Chertok, A. E. David, Y. Huang and V. C. Yang, *J. Control. Release*, **122**, 315 (2007).
120. B. Chertok, A. E. David and V. C. Yang, *J. Controlled Release*, **155**, 393 (2011).
121. T. Todd, Z. Zhen, W. Tang, H. Chen, G. Wang, Y.-J. Chuang, K. Deaton, Z. Pan and J. Xie, *Nanoscale*, **6**, 2073 (2014).
122. S. F. Medeiros, A. M. Santos, H. Fessi and A. Elaissari, *Int. J. Pharm.*, **403**, 139 (2011).
123. D. T. Nguyen, T. Charinpanitkul, D.-W. Park and K.-S. Kim, *J. Nanosci. Nanotechnol.*, In Press.
124. S. Liu, R. Xing, F. Lu, R. K. Rana and J. J. Zhu, *J. Phys. Chem. C*, **113**, 21042 (2009).
125. X. Zhang, L. Clime, H. Roberge, F. Normandin, L. H. Yahia, E. Sacher and T. Veres, *J. Phys. Chem. C*, **115**, 1436 (2011).
126. K. Cheng, S. Peng, C. Xu and S. Sun, *J. Am. Chem. Soc.*, **131**, 10637 (2009).
127. T.-Y. Liu, S.-H. Hu, T.-Y. Liu, D.-M. Liu and S.-Y. Chen, *Langmuir*, **22**, 5974 (2006).
128. S.-H. Hu, T.-Y. Liu, D.-M. Liu and S.-Y. Chen, *J. Controlled Release*, **121**, 181 (2007).
129. V. M. De Paoli, S. H. De Paoli Lacerda, L. Spinu, B. Ingber, Z. Rosenzweig and N. Rosenzweig, *Langmuir*, **22**, 5894 (2006).
130. R. Regmi, S. R. Bhattarai, C. Sudakar, A. S. Wani, R. Cunningham, P. P. Vaishnava, R. Naik, D. Oupicky and G. Lawes, *J. Mater. Chem.*, **20**, 6158 (2010).
131. T.-Y. Liu, S.-H. Hu, D.-M. Liu, S.-Y. Chen and I.-W. Chen, *Nano Today*, **4**, 52 (2009).
132. T.-Y. Liu, K.-H. Liu, D.-M. Liu, S.-Y. Chen and I.-W. Chen, *Adv. Funct. Mater.*, **19**, 616 (2009).
133. T. Hoare, J. Santamaria, G. F. Goya, S. Irusta, D. Lin, S. Lau, R. Padera, R. Langer and D. S. Kohane, *Nano Lett.*, **9**, 3651 (2009).
134. C. R. Thomas, D. P. Ferris, J. H. Lee, E. Choi, M. H. Cho, E. S. Kim, J. F. Stoddart, J. S. Shin, J. Cheon and J. I. Zink, *J. Am. Chem. Soc.*, **132**, 10623 (2010).
135. H. Huang, S. Delikanli, H. Zeng, D. M. Ferkey and A. Pralle, *Nat. Nanotechnol.*, **5**, 602 (2010).
136. R. K. Gilchrist, R. Medal, W. D. Shorey, R. C. Hanselman, J. C. Parott and C. B. Taylor, *Ann. Surg.*, **146**, 596 (1957).
137. K. Overgaard and J. Overgaard, *Eur. J. Cancer*, **8**, 65 (1972).
138. D. C. F. Chan, D. B. Kirpotin and P. A. Bunn, *J. Magn. Magn. Mater.*, **122**, 374 (1993).
139. A. Jordan, P. Wust, H. Fahling, W. John, A. Hinz and R. Felix, *Int. J. Hyperthermia*, **9**, 51 (1993).
140. M. Suzuki, M. Shinkai, H. Honda and T. Kobayashi, *Melanoma Res.*, **13**, 129 (2003).
141. A. Ito, M. Shinkai, H. Honda, K. Yoshikawa, S. Saga, T. Wakabayashi, J. Yoshida and T. Kobayashi, *Cancer Immunol. Immun.*, **52**, 80 (2003).
142. B. Sivasai, R. Rajashekar, W. Hongwang, S. N. Thilani, D. Raj-Kumar, P. Marla, K. O. Franklin, W. Brandon, L. Xiaoxuan, K. B. Olga, T. Masaaki, C. Viktor, B. H. Stefan and T. L. Deryl, *BMC Cancer*, **10**, 1 (2010).
143. R. Ivkov, S. J. DeNardo, W. Daum, A. R. Foreman, R. C. Goldstein, V. S. Nemkov and G. L. DeNardo, *Clin. Cancer Res.*, **11**, 7093s (2005).
144. S. J. DeNardo, G. L. DeNardo, A. Natarajan, L. A. Miers, A. R. Foreman, C. Gruettner, G. N. Adamson and R. Ivkov, *J. Nucl. Med.*, **48**, 437 (2007).
145. I. A. Brezovich, *Med. Phys. Monogr.*, 1682 (1988).
146. R. Hergt and S. J. Dutz, *J. Magn. Magn. Mater.*, **311**, 187 (2007).
147. E. Kita, T. Oda, T. Kayano, S. Sato, M. Minagawa, H. Yanagihara, M. Kishimoto, C. Mitsumata, S. Hashimoto, K. Yamada and N. Ohkohchi, *J. Phys. D: Appl. Phys.*, **43**, 474011 (2010).
148. G. Vallejo-Fernandez, A. G. Roca, S. Hussain, J. Timmis, V. Patel and K. O'Grady, *J. Phys. D: Appl. Phys.*, **46**, 312001 (2013).
149. C. Riviere, C. Wilhelm, F. Cousin, V. Dupuis, F. Gazeau and R. Perzynski, *Eur. Phys. J. E*, **22**, 1 (2007).
150. C. Wilhelm, J. P. Fortin and F. Gazeau, *J. Nanosci. Nanotechnol.*, **7**, 2933 (2007).
151. J. P. Fortin, F. Gazeau and C. Wilhelm, *Eur. Biophys. J.*, **37**, 223 (2008).
152. R. Hiergeist, W. Andra, N. Buske, R. Hergt, I. Hilger, U. Richter and W. Kaiser, *J. Magn. Magn. Mater.*, **201**, 420 (1999).
153. S. Mornet, S. Vasseur, F. Grasset and E. Duguet, *Mater. Chem.*, **14**, 2161 (2004).
154. S. Laurent, S. Dutz, U. O. Häfeli and M. Mahmoudi, *Adv. Colloid Interface Sci.*, **166**, 8 (2011).
155. A. E. Deatsch and B. A. Evans, *J. Magn. Magn. Mater.*, **354**, 163 (2014).
156. A. H. Habib, C. L. Ondeck, P. Chaudhary, M. R. Bockstaller and M. E. McHenry, *J. Appl. Phys.*, **103**, 07A307 (2008).
157. M. Ma, Y. Wu, J. Zhou, Y. Sun, Y. Zhang and N. Gu, *J. Magn. Magn. Mater.*, **268**, 33 (2004).
158. M. Gonzales-Weimuller, M. Zeisberger and K. M. Krishnan, *J. Magn. Magn. Mater.*, **321**, 1947 (2009).
159. M. A. Gonzalez-Fernandez, T. E. Torres, M. Andrés-Vergés, R. Costo, P. de la Presa, C. J. Serna, M. P. Moralesa, C. Marquina, M. R. Ibarra and G. F. Goya, *J. Solid State Chem.*, **182**, 2779 (2009).
160. K. H. Bae, M. Park, M. J. Do, N. Lee, J. H. Ryu, G. W. Kim, C. G. Kim, T. G. Park and T. Hyeon, *ACS Nano*, **6**, 5266 (2012).
161. A. A. Kuznetsov, O. A. Shlyakhtin, N. A. Brusentsov and O. A. Kuznetsov, *Eur. Cell. Mater.*, **3**(Suppl. 2), 75 (2002).
162. H. Hejase, S. S. Hayek, S. Qadri and Y. Haik, *J. Magn. Magn. Mater.*, **324**, 3620 (2012).
163. A. T. Apostolov, I. N. Apostolova and J. M. Wesselinova, *Eur. Phys. J. B*, **86**, 483 (2013).
164. Y. Akin, I. M. Obaidat, B. Issa and Y. Haik, Cryst. *Res. Technol.*, **44**, 386 (2009).

Kyo-Seon Kim is currently a Professor of Chemical Engineering Department at Kangwon National University, Chuncheon, Korea, where he has been working from 1989. He received the B.S., M.S. and Ph.D. degrees all in Chemical Engineering from Seoul National University, KAIST and University of Cincinnati, OH, USA in 1979, 1981 and 1989, respectively. He worked at Korea Institute of Energy and Resources as a researcher from 1981 to 1985. On his sabbatical leaves, he was a Visiting Professor at Mechanical Engineering Research Laboratory, Hitachi, Ltd, Japan during 1993-1994 and at DuPont Central Research Laboratory, USA during 2003-2004. His research interests are mainly focused on preparation and modification of nanoparticles for high-functional performances by the gas and liquid processes and also by plasma process. The main applications of nanoparticles in his researches are in the fields of medical devices, pollution control and alternative energy.